

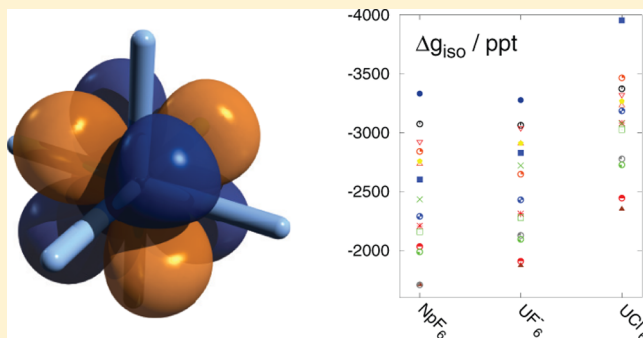
Variational versus Perturbational Treatment of Spin–Orbit Coupling in Relativistic Density Functional Calculations of Electronic g Factors: Effects from Spin-Polarization and Exact Exchange

Prakash Verma and Jochen Autschbach*

Department of Chemistry, State University of New York at Buffalo, Buffalo, New York 14260-3000

S Supporting Information

ABSTRACT: Different approaches are compared for relativistic calculations of electronic g factors of molecules with light atoms, transition metal complexes, and selected complexes with actinides, using density functional theory (DFT) and Hartree–Fock (HF) theory. The comparison includes functionals with range-separated exchange. Within the variationally stable zeroth-order regular approximation (ZORA) relativistic framework, g factors are obtained with a linear response (LR) method where spin–orbit (SO) coupling is treated as a linear perturbation, a spin-polarized approach based on magnetic anisotropy (MA) that includes SO coupling variationally, and a quasi-restricted variational SO method previously devised by van Lenthe, van der Avoird, and Wormer (LWA). The MA and LWA approaches were implemented in the open-source NWChem quantum chemistry package. We address the importance of electron correlation (DFT vs HF), the importance of including spin polarization in the g tensor methodology, the question of whether the use of nonrelativistic spin density functionals is adequate for such calculations, and the importance of treating spin–orbit coupling beyond first-order. For selected systems, the extent of the DFT delocalization error is explicitly investigated via calculations of the energy as a function of fractional electron numbers. For a test set of small molecules with light main group atoms, all levels of calculation perform adequately as long as there is no energetic near-degeneracy among occupied and unoccupied orbitals. The interplay between different factors determining the accuracy of calculated g factors becomes more complex for systems with heavy elements such as third row transition metals and actinides. The MA approach is shown to perform acceptably well for a wide range of scenarios.



1. INTRODUCTION

Valuable information about the interaction of electromagnetic fields with electric and magnetic moments of molecules can be calculated from first principles by using quantum chemical electronic structure methods. In order to faithfully treat the interaction of magnetic fields with molecular magnetic moments of the molecules, it is important to include spin–orbit (SO) coupling. This, in turn, requires a relativistic quantum theoretical framework.^{1,2}

Phenomenological spin Hamiltonians play an important role at the intersection of theory and experiment, to describe magnetic interactions of quantized spins with external and internal electromagnetic fields. An example is the electron paramagnetic resonance parameter (EPR) spin Hamiltonian

$$H = \beta_e \mathbf{B} \cdot \mathbf{g} \hat{\mathbf{S}} \quad (1)$$

which relates the energies of the observed spin transitions to an effective spin operator $\hat{\mathbf{S}}$, the external magnetic field \mathbf{B} , and a matrix \mathbf{g} which may be most appropriately called the Zeeman coupling matrix.³ β_e is the Bohr magneton. The observed g

factor for a magnetic field in the direction of a normalized vector \mathbf{q} is given by^{3,4}

$$|g| = (\mathbf{q} \cdot \mathbf{g} \mathbf{g}^T \mathbf{q})^{1/2} \quad (2)$$

with $\mathbf{G} = \mathbf{g} \mathbf{g}^T$ being a rank-2 tensor.⁵ For convenience, we refer to the Zeeman coupling matrix \mathbf{g} as the “ g tensor” (as it is usually called) despite the fact that \mathbf{g} is not a proper tensor,⁵ keeping in mind eq 2. For a free electron, the g factor is about $g_e = 2.0023$ and isotropic. The four-component (4c) relativistic Dirac equation, and exact and quasirelativistic two-component (2c) methods derived from it, imply $g_e = 2$ exactly. The deviation from 2 arises from quantum electrodynamic corrections.

In paramagnetic atoms, molecules, and metal complexes, deviations of the observed g factors from g_e , which one may refer to as g shifts in analogy to NMR chemical shifts, can be substantial because of SO coupling. Different spin states have their own characteristic EPR spectra, and the observed g

Received: November 10, 2012

factors carry important information about the electronic structure. It is therefore not surprising that the calculation of EPR g tensors of molecules and metal complexes from first principles and using semiempirical methods has a long history. Earlier attempts to get a theoretical handle on the g tensor were based on semiempirical methods; for instance, Hückel theory and variants thereof,^{6–9} or the semiempirical Hartree–Fock (HF) approximations INDO^{10–13} and CNDO.^{14–16} The connection between the spin-Hamiltonian and first-principles electronic structure theory can be made with the help of perturbation theory and the use of partitioning techniques.^{17,18} In earlier g tensor calculations, a major focus was on assessing the importance of approximations made in second order perturbation calculations,¹⁹ the problem of gauge invariance,²⁰ the importance of two-electron spin–orbit and spin–other-orbit terms,²¹ or contributions from higher order terms.²² Among the earliest g tensor calculations using HF theory and including all the spin–orbit terms as a perturbation were those by Moores and McWeeny.²³ Lushington and Grein²⁴ extended upon this work by using restricted-open shell HF (ROHF) theory and including correlation via multireference configuration interaction (MRCI). Multiconfigurational perturbation theory based on a complete-active-space reference wave function at second order (CASPT2) was used to evaluate g tensors as first order properties²⁵ using the Gerloch and McMeeking equation,²⁶ and as second-order properties^{27,28} using response theory or SOS expansions (see also ref 104). An early attempt to use effective correlated single-particle theory or density functional theory (DFT) was made by Geurts et al.²⁹ using the Slater exchange functional and uncoupled perturbation theory. Belanzoni et al.³⁰ applied generalized gradient approximation (GGA) functionals in the framework of Kohn–Sham (KS) perturbation theory. A KS-DFT linear response approach using gauge-including atomic orbitals (GIAOs) and the Pauli operator with an effective potential for spin–orbit coupling was developed by Schreckenbach and Ziegler.³¹ Malkina et al.³² obtained accurate g tensors for main-group radicals with a DFT approach that included all relevant two-electron SO terms at the Breit–Pauli level. The results were not uniformly good for heavy element systems, in particular with heavy metals. Patchkovskii and Ziegler also earlier noted problems with DFT calculations for axial $5d^1$ metal complexes.³³ For some time, accuracy issues with nonhybrid DFT magnetic property calculations have been attributed to the “uncoupled” perturbed character when solving the response equations for the external magnetic field, and sum-over-states (SOS) corrections have been suggested as a remedy.³² For further discussion see ref 34. Utilizing an effective one-electron SO operator, Neese³⁵ extended the coupled-perturbed KS DFT approach to hybrid functionals. To avoid spin-contamination in a spin-unrestricted KS approach, Rinkevicius et al.³⁶ applied spin-restricted open-shell KS linear response theory (RDFT-LR) to obtain electronic g tensors for a set of main group organic radicals. The RDFT-LR formalism produced g tensors for organic radicals consistent with MR-CI except for anions, where spin polarization becomes vital. Rinkevicius et al.³⁷ corrected the shortcomings of the spin-restricted method by introducing spin-polarization in a “restricted-unrestricted” approach.³⁸ An assessment of the performance of a SOS approach to obtain the g tensor with wave function methods can be found in ref 40. Gilka et al.³⁹ studied the case of AlO where, due to a near-degeneracy of excited states at certain

interatomic distances, results from a SOS formalism were unreliable.

In order to include SO coupling to higher orders in g tensor calculations, van Lenthe, van der Avoird, and Wormer (LWA)⁴¹ developed a quasi spin-restricted DFT GIAO approach for Kramers doublets where SO coupling is included variationally in the ground state. In this case, the g tensor is obtained from matrix elements of the Zeeman Hamiltonian in a basis of a Kramers pair of orbitals, which goes back to a prescription by Abragam and Bleaney.⁵ Neyman et al.⁴² developed a similar approach using the Douglas–Kroll–Hess (DKH) Hamiltonian and a restricted open-shell Kohn–Sham framework. A somewhat related, spin-polarized method for g tensor calculations with generalized HF theory has been introduced by Jayatilaka,⁴³ where a quantization axis (c.f. eq 2) can be defined via a finite magnetic field. More recently, Kaupp et al.^{44,45} have put forward two-component DFT methods for calculating EPR parameters, where different M_J states are prepared variationally by aligning the magnetic moments of electrons ascribed to the total electronic angular momentum \mathbf{J} along different directions. Part of the Zeeman coupling matrix is obtained from the calculations for a given orientation.

Much of the early work on g tensors was based on the Pauli (or Breit–Pauli) operator, which, however, is not variationally stable and affords numerically problematic terms in higher orders and/or in calculations of certain molecular properties. The past two decades have seen tremendous progress of the development of variationally stable methods utilizing “fully relativistic” 4-component (4c) theory, approximate 2-component (2c) “quasirelativistic” Hamiltonians, and more recently, exact 2c operators. Recent summaries of the developments in this field can be found, for example, in refs 46–49. An important topic of research remains the simultaneous treatment of correlation and relativity in a computationally efficient manner. In principle, DFT provides an effective solution of the correlation problem, but in practice the performance of approximate functionals for specific purposes requires careful testing. Much work remains to be done regarding the development of well-performing relativistic functionals⁵⁰ and a treatment of open-shell systems with strong multireference character in KS DFT. Regarding relativistic effects, for molecular properties that depend predominantly on valence orbitals, the variationally stable zeroth-order regular approximation (ZORA)⁵¹ is established as an accurate quasirelativistic method. Magnetic perturbation operators are straightforwardly derived within this framework, and it is conceptually simple and computationally efficient to obtain their matrix elements by numerical integration or by using a combination of analytical and numerical techniques.^{41,51–58}

The present work is concerned with a side-by-side comparison of different conceptual approaches by which electronic g factors (or g shifts) can be obtained from variational relativistic DFT and HF calculations. Calculations are performed within the ZORA relativistic framework on a benchmark set comprised of molecules and complexes with main group atoms, light and heavy transition metals, and actinides. For consistency, the same basis sets, functionals, and integration grids are employed for different types of g shift calculations on a given system, and all calculations are performed with the same electronic structure code: the open-source NWChem package.⁵⁹ The g shift calculations differ in the way that SO coupling and spin-polarization are treated. A comparison is made between the following: (i) Linear

Response (LR) calculations where SO coupling is not included in the ground state electronic structure but treated as a perturbation when evaluating the g shifts. A LR ZORA implementation for g shifts in NWChem, utilizing GIAOs, was recently carried out by our group.⁵⁵ (ii) The Kramers-doublet method devised by van Lenthe, Wormer, and Avoird (LWA)⁴¹ where SO coupling is treated variationally in a quasi-restricted setup described in section 2.1. A new ZORA GIAO-based implementation of the LWA formalism in NWChem is reported herein. (iii) Variational SO calculations with different orientations of the spin-quantization axis, by which the g tensor is extracted from matrix elements of the Zeeman Hamiltonian calculated from DFT calculations converged with different spin quantization directions. The latter method is inspired by, and closely related to, recently published work by van Wüllen et al. on the calculating zero-field splitting (ZFS) and magnetic anisotropy (MA)^{60,61} and therefore herein referred to as the “MA” approach. See also presentation notes by van Wüllen where the calculation of ZFS and g matrices is discussed.⁶² Conceptually, there are also close similarities to the variational SO g tensor approaches mentioned above. Functionality for the required generalized-collinear SO DFT ZORA calculations has been implemented in NWChem to enable g tensor calculations within the MA framework.

In a recent paper, Hrobarik et al. noted large differences in calculated g shifts when treating SO coupling beyond a first-order perturbation.⁴⁵ Their report motivated us to study higher-order SO effects with a g shift benchmark molecule set extended from ref 55 and to evaluate the MA and LWA approaches and the role of spin-polarization in this context. We investigate the performance of “pure” (nonhybrid) functionals, global hybrid functionals, and hybrids with range-separated exchange in the different types of calculations, and we compare DFT with HF theory. Further, the importance of using a distributed gauge-origin formalism is assessed.

Section 2 summarizes some theoretical aspects regarding the LR, LWA, and MA calculations of g tensors within the ZORA-DFT framework. Computational details are provided in section 3. Results for a benchmark set of molecules and metal complexes with light to very heavy atoms are reported and discussed in section 4. Concluding remarks can be found in section 5.

2. THEORY

Hartree atomic units with $e = 1$, $m_e = 1$, $\hbar = 1$, $4\pi\epsilon_0 = 1$, $c = \alpha^{-1} \approx 137.036$ are used throughout this section unless explicitly noted otherwise.

2.1. Two-Component DFT Calculations. In the calculations with SO coupling included variationally, self-consistent field (SCF) solutions for the two-component Kohn–Sham (KS) equations expressed in an atomic orbital (AO) basis set $\{\chi_\mu\}$ are obtained from

$$\begin{pmatrix} \mathbb{F}^{\alpha\alpha} & \mathbb{F}^{\alpha\beta} \\ \mathbb{F}^{\beta\alpha} & \mathbb{F}^{\beta\beta} \end{pmatrix} \begin{pmatrix} \mathbf{C}^\alpha \\ \mathbf{C}^\beta \end{pmatrix} = \begin{pmatrix} \mathbb{S} & 0 \\ 0 & \mathbb{S} \end{pmatrix} \begin{pmatrix} \mathbf{C}^\alpha \\ \mathbf{C}^\beta \end{pmatrix} \epsilon \quad (3)$$

subject to the MO orthonormality condition $\mathbf{C}^\dagger \mathbb{S} \mathbf{C} = \mathbf{1}$. The notation $\mathbf{C}^\dagger \dots \mathbf{C}$ implies summation over spin indices. In eq 3, \mathbb{F} is the complex AO matrix of the two-component KS Fock operator $\hat{F} = \hat{h} + V_C + V_{XC}$, and \mathbb{S} is the AO overlap matrix. The operator \hat{h} is the one-electron part of \hat{F} , V_C is the electronic Coulomb potential, and V_{XC} is the exchange-correlation (XC)

potential, the nonlocal exact exchange in HF theory, or a hybrid thereof. The matrices \mathbf{C}^γ collect the molecular orbital (MO) coefficients for the spin- γ components of the MOs, and ϵ is a diagonal eigenvalue matrix (orbital energies). Within the ZORA framework, the field-free one-electron part $\hat{h}^{(0)}$ of the Fock operator reads

$$\hat{h}^{(0)} = V_{\text{ext}} + \frac{1}{2}(\boldsymbol{\sigma} \cdot \hat{\mathbf{p}}) \mathcal{K} (\boldsymbol{\sigma} \cdot \hat{\mathbf{p}}) \quad (4)$$

where V_{ext} is the external potential from the atomic nuclei, $\boldsymbol{\sigma}$ is the three-vector of the Pauli spin matrices, $\hat{\mathbf{p}} = -i\nabla$ is the linear momentum operator, and

$$\mathcal{K} = \frac{2c^2}{2c^2 - V} \quad (5)$$

In this work, the DFT component of V_{XC} is based on a nonrelativistic XC spin-density functional that is evaluated with the relativistic density and a suitably defined spin magnetization. The potential V in eq 5 is in principle the same as the effective potential $V_{\text{ext}} + V_C + V_{XC}$ in the SCF procedure. In practice, V is approximated as V_{ext} plus a sum of atomic electronic Coulomb potentials,⁵⁴ which is also used as an initial guess for the SCF. The computations are performed with an odd number of electrons $N = 2n + 1$, either in spin-polarized form with an odd number of singly occupied one- or two-component orbitals, or in the form of quasi-restricted KS calculations. The latter method produces orbitals that come in degenerate pairs, by assigning single occupancy to the lowest energy $2n$ orbitals and an occupancy of 1/2 to the orbitals $(2n + 1)$ and $(2n + 2)$. For example, for HgH with 81 electrons, the quasi-restricted approach gives 80 spin-orbitals with full occupancy while orbitals 81 and 82 are assigned half occupancy, and either one can be used as the unpaired orbital (“singly occupied MO” or SOMO) for the LWA-type calculations of the g tensor described in section 2.3.

In the LR calculations of the g tensor, SO coupling is treated as a perturbation. A spin-unrestricted SCF calculation is in this case performed with the scalar part of the ZORA operator

$$\hat{h}_{\text{scalar}}^{(0)} = V_{\text{ext}} + \frac{1}{2} \hat{\mathbf{p}} \mathcal{K} \hat{\mathbf{p}} \quad (6)$$

while

$$\hat{h}_{\text{SO}} = \frac{i}{2} \boldsymbol{\sigma} \cdot (\hat{\mathbf{p}} \mathcal{K} \times \hat{\mathbf{p}}) \quad (7)$$

is used in conjunction with the Zeeman operator for a double-perturbation (linear response) calculation of the g shift. The LR implementation in NWChem for g factor calculations with GIAOs has been described in ref 55.

2.2. Field-Dependent Terms. The one-electron ZORA Zeeman (Z) operator, describing the terms linear in an external magnetic field \mathbf{B} , can be written as^{41,55,63}

$$\hat{h}^Z = \frac{1}{4} [\mathbf{B} \cdot (\mathbf{r} \times \hat{\mathbf{p}} \mathcal{K}) + \mathbf{B} \cdot (\mathbf{r} \times \mathcal{K} \hat{\mathbf{p}}) + \boldsymbol{\sigma} \cdot \{\mathbf{B} (\nabla \cdot \mathcal{K} \mathbf{r}) - (\mathbf{B} \cdot \nabla) \mathcal{K} \mathbf{r}\}] \quad (8)$$

The notation $\{\dots\}$ indicates that derivatives in the spin-dependent part are acting only on \mathbf{r} and \mathcal{K} inside the operator. For calculations of magnetic-field perturbations, the derivative operator

$$\hat{h}_u^Z = \frac{\partial \hat{h}^Z}{\partial B_u} = \frac{1}{4} \left[(\mathbf{r} \times \hat{\mathbf{p}} \mathcal{K})_u + (\mathbf{r} \times \mathcal{K} \hat{\mathbf{p}})_u + \left(\frac{g_e}{2} \sigma_u \{ \nabla \cdot \mathcal{K} \mathbf{r} \} - \sigma \cdot \{ \nabla_u \mathcal{K} \mathbf{r} \} \right) \right] \quad (9)$$

is needed, with u being x , y , or z . In numerical integrations used to obtain matrix elements of \hat{h}_u^Z , partial integration can be used to avoid evaluating derivatives of \mathcal{K} . Matrix elements in the AO basis are evaluated numerically using the same grids that are used in evaluating matrix elements of $\hat{h}^{(0)}$ and matrix elements of the XC energy functional and potential. For further details please see ref 55. A factor $g_e/2$ has been introduced in the spin-dependent part of eq 9 in order to ensure that in the limit of vanishing SO coupling the free electron g value is recovered. See section 2.4 for further details.

2.3. Implementation of the g Tensor Following the LWA Approach. Following LWA⁴¹ (going back to a discussion in ref 5), the Fock operator up to first order in the field \mathbf{B} is expressed in the basis of one of the SOMO orbitals of the quasi-restricted SCF calculation and its Kramers conjugate. The expression is subsequently interpreted as a matrix representation of the EPR spin-Hamiltonian in eq 1. The matrix \mathbf{g} is then extracted directly from field derivatives of the matrix elements. Either one of the orbitals with half occupancy from a quasi-restricted calculation can be designated as the SOMO φ , which is one member, Φ_1 , of a Kramers pair. Its Kramers conjugate Φ_2 is obtained by applying the time-reversal operator, $\Phi_2 = -i\sigma_y \hat{K}_0 \Phi_1$. Here, \hat{K}_0 is an antilinear operator that converts an orbital into its complex conjugate.¹ Explicitly written in terms of the spin components separated into real (R) and imaginary (I) parts of the SOMO, the pair reads

$$\Phi_1 = \begin{pmatrix} \varphi_\alpha^R \\ \varphi_\beta^R \end{pmatrix} + i \begin{pmatrix} \varphi_\alpha^I \\ \varphi_\beta^I \end{pmatrix} \quad (10a)$$

$$\Phi_2 = \begin{pmatrix} -\varphi_\beta^R \\ \varphi_\alpha^R \end{pmatrix} + i \begin{pmatrix} \varphi_\beta^I \\ -\varphi_\alpha^I \end{pmatrix} \quad (10b)$$

The matrix elements of the field-dependent Fock operator are calculated in the basis $\{\Phi_1, \Phi_2\}$, and elements of the matrix \mathbf{g} are extracted for the Kramers doublet ($S = 1/2$) as

$$\begin{aligned} g_{ux} &= \frac{1}{\beta_e S} \text{Re} \frac{\partial}{\partial B_u} \langle \Phi_1 | \hat{F} | \Phi_2 \rangle = \frac{1}{\beta_e S} \text{Re} \frac{\partial}{\partial B_u} \langle \Phi_2 | \hat{F} | \Phi_1 \rangle \\ g_{uy} &= -\frac{1}{\beta_e S} \text{Im} \frac{\partial}{\partial B_u} \langle \Phi_1 | \hat{F} | \Phi_2 \rangle = \frac{1}{\beta_e S} \text{Im} \frac{\partial}{\partial B_u} \langle \Phi_2 | \hat{F} | \Phi_1 \rangle \\ g_{uz} &= \frac{1}{\beta_e S} \text{Re} \frac{\partial}{\partial B_u} \langle \Phi_1 | \hat{F} | \Phi_1 \rangle = -\frac{1}{\beta_e S} \text{Re} \frac{\partial}{\partial B_u} \langle \Phi_2 | \hat{F} | \Phi_2 \rangle \end{aligned} \quad (11)$$

The derivation assumes that the KS orbitals minimize the energy functional. The derivatives are only taken with terms in the Φ_i and in \hat{F} that explicitly depend on \mathbf{B} (not implicitly, for instance, via the magnetic-field dependence of the MO coefficients). The derivatives here and elsewhere in this article are understood to be taken at $\mathbf{B} = 0$. The operator \hat{F} is the Fock operator to first order in the field, $\hat{F}(\mathbf{B})$, with \hat{h}^Z from eq 8 being its one-electron part. The orbitals may also be explicitly field-dependent (see the Appendix for details). Assuming a

complete basis, or a basis set that is not dependent on the magnetic field amplitude, by virtue of the Hellmann–Feynman theorem, the matrix elements in eq 11 simplify as

$$\frac{\partial}{\partial B_u} \langle \Phi_i(\mathbf{B}) | \hat{F}(\mathbf{B}) | \Phi_j(\mathbf{B}) \rangle = \langle \Phi_i | \hat{h}_u^Z | \Phi_j \rangle \quad (12)$$

with \hat{h}_u^Z given in eq 9 and the Φ_i on the right-hand side are field-independent MOs.

2.4. Implementation of the g Tensor Following the MA Approach. A row of the g matrix can alternatively be obtained with a DFT approach originally devised by van Wüllen et al. for zero-field splitting (ZFS).^{60–62} Because of the relation to the magnetic anisotropy, we refer to this approach as MA. It is suitable for spin-polarized calculations. The ZFS calculations rest on a dependence of the energy on the chosen spin-quantization direction in a generalized-collinear DFT calculation with SO coupling variationally included. Other spin-dependent properties can be obtained in a similar fashion. The following is meant to be an illustration of the protocol rather than a derivation. Consider an expectation value of the EPR spin-Hamiltonian (eq 1) for spin $S = 1/2$ taken with the KS determinant

$$\begin{aligned} E(\mathbf{q}, \mathbf{B}) &= \sum_i n_i \langle \varphi_i^q | \beta_e \mathbf{B} \cdot \hat{\mathbf{g}} | \varphi_i^q \rangle \\ &= \beta_e \sum_{uv} g_{uv} B_u \sum_i n_i \langle \varphi_i^q | \hat{S}_v | \varphi_i^q \rangle \end{aligned} \quad (13)$$

where $u, v \in \{x, y, z\}$. In the previous equation, the φ_i^q are the two-component KS orbitals obtained from a generalized collinear DFT calculation with selected spin-quantization axis \mathbf{q} , and the n_i are the occupation numbers. For convenience, \mathbf{q} is assumed to be a normalized vector. With pure spin-eigenfunctions, one finds

$$\sum_i n_i \langle \varphi_i^q | \mathbf{q} \cdot \hat{\mathbf{S}} | \varphi_i^q \rangle = S = (n_\alpha - n_\beta)/2 \quad (14)$$

Here, n_γ is the sum of occupations of orbitals with positive ($\gamma = \alpha$) or negative ($\gamma = \beta$) projection along the chosen quantization axis. Now choose \mathbf{q} parallel to one of the coordinates v . The derivative of the right-hand side of eq 13 with respect to a component B_u of the magnetic field gives, with eq 14,

$$\frac{\partial E(v, \mathbf{B})}{\partial B_u} = \beta_e S g_{uv} \quad (15)$$

In a generalized collinear Kohn–Sham DFT calculation with SO coupling, one obtains to first order in the magnetic field

$$\frac{\partial E(v, \mathbf{B})}{\partial B_u} = \sum_i n_i \frac{\partial}{\partial B_u} \langle \varphi_i^v | \hat{F} | \varphi_i^v \rangle \quad (16)$$

where the Fock operator and the orbitals can be field dependent. If there is magnetic anisotropy, the energy calculated in the absence of the field, $E(v, 0)$, is dependent on the choice of the spin-quantization direction v . It follows from a comparison of eq 15 with eq 16

$$g_{uv} = \frac{1}{\beta_e S} \sum_i n_i \frac{\partial}{\partial B_u} \langle \varphi_i^v(\mathbf{B}) | \hat{F}(\mathbf{B}) | \varphi_i^v(\mathbf{B}) \rangle \quad (17)$$

Derivative terms that depend on the magnetic field via the basis functions are provided in the Appendix. With a complete basis, or with a basis set that is independent of the magnetic field amplitudes,

$$g_{uv} = \frac{1}{\beta_e S} \sum_i n_i \langle \varphi_i^v | \hat{h}_u^Z | \varphi_i^v \rangle \quad (18)$$

with \hat{h}_u^Z defined in eq 12, and field-free orbitals φ_i^v .

In a “nonrelativistic limit with spin,” the magnetic field derivative of the Zeeman Hamiltonian reads

$$\frac{\partial \hat{h}_{\text{nr}}^Z}{\partial B_u} = \frac{1}{2} (\mathbf{r} \times \hat{\mathbf{p}})_u + \frac{g_e}{2} \hat{S}_u \quad (19)$$

In the ZORA framework, this expression is obtained from eq 9 upon letting $\mathcal{K} \rightarrow 1$. The two-component KS orbitals can be chosen in such a calculation as pure spin orbitals, as in eq 14, with real spatial components. Since $\mathbf{r} \times \hat{\mathbf{p}}$ is imaginary, the diagonal matrix elements of this operator in a basis of real spatial functions are zero. With $\beta_e = 1/2$ au, eq 18 then works out as $g_{uv} = g_e \delta_{uv}$ which corresponds to the isotropic free-electron case. With SO coupling present, the orbitals are no longer pure spin orbitals, and they may acquire imaginary components in their spatial functions. In this case, deviations from the free-electron g factor manifest themselves in the calculation.

3. COMPUTATIONAL DETAILS

The test set comprises the molecules CH_3 , HCO , HSiO , HSiS , SiOH , SiSH , TiF_3 , TcNCl_4^- , ReNCl_4^- , HgH , HgF , NpF_6 , UF_6^- , and UCl_6^- . Subset 1 (CH_3 , HCO , HSiO , HSiS , SiOH , and SiSH) only has relatively light main group elements. Subset 2 (HgH , HgF , TiF_3 , TcNCl_4^- , and ReNCl_4^-) includes light and heavy transition elements, while subset 3 (NpF_6 , UF_6^- , UCl_6^-) includes actinides. The g tensor calculations were performed using a locally modified version of NWChem. Results are reported in terms of g shifts, $\Delta g = g - g_e$, and g shift tensor components, in parts per thousand (ppt).

For C, H, N, O, F, Si, S, and Cl, the IGLO-III⁶⁸ basis was used. An uncontracted ANO-RCC basis^{69,70} was used for Ti, Hg, Tc, Re, U, and Np. g functions were removed from the Hg basis, and h functions were removed from the Ti, Np, and U basis sets, since we found in previous work that these functions in the ANO basis sets are not having much of an effect in DFT calculations of various molecular properties.^{55,57,58,71} The following density functionals were applied for this work: Becke-88 exchange + Perdew-86 correlation (BP)^{72,73} and the three-parameter hybrid B3PW91⁷⁴ with 20% nonlocal exact exchange, for comparing results for TcNCl_4^- and ReNCl_4^- with ref 45, the Perdew–Burke–Ernzerhof (PBE) functional,⁷⁵ a hybrid version of PBE with 25% nonlocal exact exchange (PBE0),⁷⁶ a “coulomb attenuated” range-separated hybrid functional with 19% nonlocal exact exchange at short interelectronic separations and 65% asymptotically (CAM-B3LYP, or short CAM),⁷⁷ and a long-range (LR) corrected range-separated hybrid based on PBE0 with 25% nonlocal exact exchange at short interelectronic separations and 100% asymptotically (LC-PBE0).⁷⁸ Additional calculations were carried out at the HF level.

Optimized geometries for CH_3 , HCO , HSiO , HSiS , SiOH , SiSH , HgH , HgF , and TiF_3 were taken from ref 55 (optimized with the ADF⁷⁹ program with scalar ZORA, the BP functional, and a triple- ζ doubly polarized (TZ2P) Slater-type basis). Optimized CASSCF and CASPT2 geometries for NpF_6 , UF_6^- , and UCl_6^- were taken from ref 80. Experimental geometries for the complexes TcNCl_4^- and ReNCl_4^- were taken from refs 81 and 82, respectively.

In most cases, the g shifts are on the order of a few to a few hundred ppt, and therefore the calculated g factors can safely be considered as positive. The sign of the g shift tensor components (see eq 2 and the text following the equation) is then unambiguous. For the LR results, we calculate the g shifts directly (see ref 55), and the signs of the components are reported as calculated. For the LWA and MA calculations, we form the matrix \mathbb{G} , obtain the g factors g_i , $i = 1 - 3$, as the square roots of the eigenvalues, and then assign the g shifts. As pointed out by Abragam and Bleaney,⁵ the sign of the determinant of the Zeeman coupling matrix \mathbf{g} gives the sign of the product $g_1 g_2 g_3$. For example, for the actinide halides investigated here, most calculations give a negative sign for the product. Since the three g factors of these systems are equal due to symmetry, they must therefore be negative. In such a case, the g shifts reported herein are based on negative g factors. The ordering adopted in the data tables of Section 4 is for the g shift tensor principal components, with $\Delta g_1 \leq \Delta g_2 \leq \Delta g_3$. The isotropic g shift is given as the average $\Delta g_{\text{iso}} = (1/3) \sum_i \Delta g_i$. For systems with axial symmetry, we report instead the g shift tensor components parallel (\parallel) and perpendicular (\perp) to the principal symmetry axis of the molecule, along with Δg_{iso} .

4. RESULTS AND DISCUSSION

4.1. Basis Set Truncation and GIAOs. For incomplete basis sets, the g tensor, like other calculated magnetic properties that involve external magnetic fields, is dependent on the chosen origin of the magnetic vector potential. Depending on the flexibility of the basis set used, and the type of property, in practical computations, this problem can range from severe to barely noticeable. In general, the less flexible the basis set is, the more severe becomes the origin dependence. For instance, magnetizabilities are very strongly origin dependent.^{83,84} In variational quantum chemical methods such as DFT, the origin dependence of magnetic properties is effectively eliminated by using a GIAO basis set or another type of distributed gauge-origin method, which also tends to improve results toward the basis set limit. Reference 85 shows a rather dramatic case of slow convergence of the proton NMR shielding in the HF molecule with the basis set size when GIAOs are not employed.

Previously, van Lenthe et al. (LWA) numerically demonstrated a minor origin dependence of g shifts in their calculations,⁴¹ but only for systems with relatively light elements. In order to investigate the origin dependence of g -shifts obtained with this method in our calculations we adopted the LWA approach in a pure DFT setup which simplifies the implementation somewhat (see Appendix). Calculations were performed with the coordinate origin at the center of nuclear charges (CNC), and with the CNC located at (30, 30, 30) Å. The basis sets adopted for most calculations in this report are flexible enough such that the translation of the coordinate axis has a very small effect on the g shifts (see Supporting Information (SI)). However, with a somewhat smaller basis set such as SARC-ZORA for the heavy atoms, a more pronounced origin dependence of the g shifts is observed. Table 1 shows representative results for HgH and ReNCl_4^- . The largest effect is seen for Δg_{\perp} of ReNCl_4^- where the origin dependence is of similar magnitude to the g shift itself. The GIAO formalism is seen to give the expected origin invariance. Minor deviations between the unshifted and the shifted GIAO results are a consequence of the large coordinate displacement needed to bring about noticeable origin-dependence effects, in con-

Table 1. Origin Dependence of g Shifts (in ppt)^a

		coordinate center (0, 0, 0)		coordinate center (30, 30, 30)	
		AO basis	GIAOs	AO basis	GIAOs
HgH	Δg_{\parallel}	-24.9	-24.9	-18.7	-24.9
	Δg_{\perp}	-238.5	-239.6	-225.5	-240.7
	Δg_{iso}	-167.3	-168.1	-156.7	-168.7
ReNCl ₄ ⁻	Δg_{\parallel}	-39.6	-38.8	-32.5	-38.8
	Δg_{\perp}	-79.5	-76.8	-116.3	-76.8
	Δg_{iso}	-66.2	-64.1	-88.3	-64.1

^aLWA approach, PBE functional, and SARC-ZORA basis⁸⁶ for heavy metal atoms.

junction with the limited accuracy of the numerical integration used to obtain some of the operator matrix elements.

4.2. Assessment Strategies. In the comparison of the different methods, it is important to keep in mind their particular differences and similarities. The LR approach includes spin-polarization and scalar relativistic effects variationally, while SO coupling is treated perturbatively at lowest order. Both the LWA and the MA approaches include SO coupling variationally and therefore afford higher order SO effects in the calculated results. The main difference between LWA, as implemented here, and MA is that the latter includes spin polarization. We therefore use comparisons of LR and MA to gauge the impact of SO coupling beyond lowest order and comparisons of LWA and MA to investigate the importance of spin polarization.

Comparisons between HF and DFT calculations provide information about the importance of electron correlation. However, DFT calculations with approximate functionals also afford deficiencies—other than an incomplete treatment of correlation—which tend to have adverse effects on the quality of the results. An example is the DFT delocalization error⁸⁷ that tends to produce chemical bonds with a too high degree of covalency. Another issue is the treatment of spin polarization. The nonlocal HF exchange operator contributes both to the

diagonal and the off-diagonal spin blocks of the Fock matrix in eq 3, and spin polarization may therefore take an effect on the various contributions. A relativistic XC functional and calculated magnetic properties should depend on a four-current⁵⁰ $\mathbf{J} = (\rho, c^{-1}\mathbf{j})$, where \mathbf{j} is the current density which has an orbital-current and a spin magnetization component (ρ the electron density), and in two-component form presumably also contribute to all spin blocks in the KS Fock operator. Nonrelativistic approximate spin-density functionals such as PBE are frequently used in relativistic calculations with the help of a suitable definition of a spin magnetization (e.g., in the generalized collinear or noncollinear approximations). Hence, there are approximations in DFT when it comes to the treatment of exchange, spin polarization, and magnetic properties in relativistic calculations with common non-relativistic spin density functionals, which is likely to have adverse effects on properties of open-shell systems such as the g tensor. Another potential issue is the use of the KS density matrix in such a framework, in place of the density matrix of the interacting system.

4.3. Doublet Radicals with Light Atoms. For doublet radicals with light(er) elements (H, C, O, Si, S; test set #1), data obtained with different approaches for the g tensor, and with different functionals, are collected in Tables 2 (HF, PBE, PBE0) and 3 (hybrid functionals with range-separated exchange). Scatter-plots of the calculated isotropic g shifts, including the results for molecule sets #2 and #3 that are discussed in subsequent sections, are shown in Figure 1.

Overall, the MA approach produces g shifts that are equivalent to LR. All three methods (viz. LR, MA, and LWA) in fact provide similar g shifts, with the exception of SiOH and SiSH. For these two molecules, LWA produces g shifts that are far out of the range predicted by the other two methods. We also notice a larger discrepancy between LR and MA for these two molecules. We discuss these systems below, after an overall assessment of the calculations.

HF and DFT produce somewhat comparable results. For the g shifts of the light atomic radical set, electron correlation does

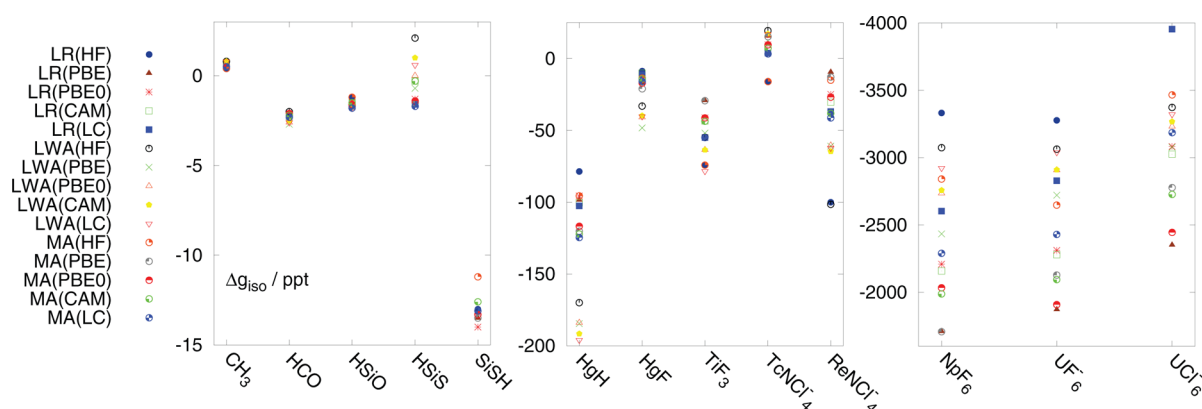
Table 2. g Shifts (in parts per thousand) for Molecule Set #1, with Light Main-Group Atoms^a

		HF				PBE				PBE0			
		Δg_1	Δg_2	Δg_3	Δg_{iso}	Δg_1	Δg_2	Δg_3	Δg_{iso}	Δg_1	Δg_2	Δg_3	Δg_{iso}
CH ₃	LR	0.0	0.6	0.6	0.4	0.0	0.8	0.8	0.5	0.0	0.8	0.8	0.5
	MA	0.0	0.6	0.6	0.4	0.0	0.8	0.8	0.5	0.0	0.8	0.8	0.5
	LWA	0.0	1.2	1.2	0.8	0.0	1.1	1.1	0.7	0.0	1.1	1.1	0.7
HCO	LR	-8.6	-0.4	2.7	-2.1	-9.1	-0.1	2.8	-2.1	-9.1	-0.1	2.8	-2.1
	MA	-8.6	-0.4	2.7	-2.1	-9.1	-0.2	2.8	-2.1	-9.1	-0.2	2.9	-2.1
	LWA	-9.5	0.1	3.4	-2.0	-11.4	-0.1	3.2	-2.7	-11.0	0.0	3.3	-2.6
HSiO	LR	-8.4	0.7	4.1	-1.2	-9.9	0.1	4.7	-1.7	-9.7	0.2	4.8	-1.6
	MA	-8.4	0.6	4.1	-1.2	-9.9	0.0	4.8	-1.7	-9.7	0.2	4.9	-1.6
	LWA	-9.9	-0.2	4.9	-1.7	-11.0	0.1	6.2	-1.5	-10.7	0.0	6.1	-1.5
HSiS	LR	-18.3	-0.5	14.0	-1.6	-21.7	-0.5	17.6	-1.5	-21.0	-0.4	17.4	-1.3
	MA	-18.5	-0.6	13.9	-1.7	-21.6	-0.7	17.6	-1.5	-20.9	-0.5	17.4	-1.4
	LWA	-16.3	0.9	21.8	2.1	-23.4	-0.3	21.6	-0.7	-21.7	-0.1	21.8	0.0
SiOH	LR	-58.3	-1.8	0.4	-19.9	-68.4	-2.6	-0.1	-23.7	-73.0	-2.3	0.0	-25.1
	MA	-38.5	-1.7	0.3	-13.3	-68.6	-2.5	-0.1	-23.7	-61.1	-2.1	0.0	-21.1
	LWA	-10.9	-9.5	189.0	56.2	-395.2	-40.2	-43.7	-159.7	-744.5	-146.5	-149.6	-346.9
SiSH	LR	-40.2	-1.6	2.8	-13.0	-42.3	-1.5	3.2	-13.5	-45.2	-1.4	3.4	-14.4
	MA	-34.9	-1.7	2.9	-11.2	-42.2	-1.6	3.4	-13.5	-41.9	-1.4	3.5	-13.3
	LWA	-256.9	-19.1	-11.3	-95.8	-82.7	-1.9	3.3	-27.1	-92.9	-2.5	3.5	-30.6

^aHF theory and DFT with the PBE and PBE0 functionals.

Table 3. g Shifts (in parts per thousand) for Molecule Set #1, with Light Main-Group Atoms^a

		CAM-B3LYP				LC-PBE0			
		Δg_1	Δg_2	Δg_3	Δg_{iso}	Δg_1	Δg_2	Δg_3	Δg_{iso}
CH ₃	LR	0.0	0.8	0.8	0.5	0.0	0.8	0.8	0.5
	MA	0.0	0.8	0.8	0.5	0.0	0.8	0.8	0.5
	LWA	0.0	1.2	1.2	0.8	0.0	1.2	1.2	0.8
HCO	LR	−9.3	−0.1	2.9	−2.2	−9.8	−0.2	2.9	−2.3
	MA	−9.3	−0.1	2.9	−2.2	−9.7	−0.2	2.9	−2.3
	LWA	−10.9	0.0	3.3	−2.5	−11.3	0.0	3.3	−2.6
HSiO	LR	−9.8	0.4	5.1	−1.5	−10.1	0.2	4.7	−1.7
	MA	−9.8	0.4	5.1	−1.5	−10.2	0.2	4.7	−1.8
	LWA	−10.7	0.0	5.9	−1.6	−10.9	0.0	5.7	−1.8
HSiS	LR	−20.6	0.2	19.5	−0.3	−22.1	−0.4	17.7	−1.6
	MA	−20.7	0.1	19.6	−0.3	−22.4	−0.5	17.8	−1.7
	LWA	−20.5	0.1	23.3	1.0	−20.8	0.1	22.5	0.6
SiOH	LR	−103.7	−2.6	0.1	−35.4	−106.3	−2.1	0.1	−36.1
	MA	−60.4	−2.4	0.1	−20.9	−59.2	−1.9	0.1	−20.3
	LWA	−251.3	−249.7	956.6	151.8	−40.8	−39.1	387.7	102.6
SiSH	LR	−56.5	−0.8	3.6	−17.9	−58.9	−1.2	4.0	−18.7
	MA	−40.7	−0.8	3.7	−12.6	−42.1	−1.2	4.1	−13.1
	LWA	−85.0	−2.1	4.3	−27.6	−94.2	−2.6	4.9	−30.7

^aHybrid density functionals with range-separated exchange.**Figure 1.** Isotropic g shifts (Δg , in ppt) for molecules sets #1 to #3, calculated with different methods. In the plot key, CAM = CAM-B3LYP, LC = LC-PBE0. For the Si-containing radicals, some of the LWA data lie outside of the plot range.

not appear to play an outstanding role. Moreover, differences among the XC functionals lead to relatively minor differences in the calculated g shift data. LC-PBE0 does not outperform the other density functionals. The wrong asymptotic behavior of most approximate XC potentials (including CAM-B3LYP) therefore has no adverse effects in DFT calculations of the g tensors of molecule set #1. Spin polarization is of some significance, as the differences between LR and MA versus LWA indicate. However, with the exception of SiOH and SiOS, these differences are on par, in terms of magnitude, with the variations of the results among different functionals and HF. Higher order spin–orbit effects (from a variational treatment of SO coupling in the MA and LWA methods) are, as one may have expected, not of much relevance for the light atomic radicals. The LR calculations provide almost identical g shifts to those in the MA approach. We forego a comparison with experimental values for set #1 and refer the reader to our previous paper which reported the LR implementation and comparisons with experimental data.⁵⁵

Regarding the SiOH and SiSH cases, based on a preliminary comparison of nonhybrid DFT LR versus LWA calculations⁸⁸

(PBE functional), it has been noted previously that a large overestimation of the isotropic g shift magnitude of SiOH (−135 ppt obtained with the LWA ZORA implementation in the ADF code, vs −24 ppt in spin-polarized calculations, similar to the PBE results listed in Table 2) may be indicative of the importance of spin-polarization in the formalism. As in our present calculations, the g shift tensor span in the spin-restricted LWA calculations was also very large, over 300 ppt. For the molecule SiSH, the isotropic LWA g shift was reported in ref 88 as −29 ppt, which compares well with our PBE result of −27 ppt. The comparison with other functionals shows that LWA/PBE gives a fortuitously “small” Δg_{iso} for this system, although it is already a factor of 2 too large compared to LR and MA. With the other functionals, the LWA calculations on SiSH are clearly identified as outliers. The data collected here for individual tensor components, with a range of density functionals and HF, and the comparison with the spin-polarized MA approach casts some doubt on the idea that it is the lack of spin polarization as such that is causing poor results. For SiOH and SiSH, the quasi-restricted calculations lead to very small HOMO–LUMO gaps (the energy gap between the doubly

Table 4. *g* Shifts (in parts per thousand) for Molecule Set #2, with Main-Group and Transition Metal Atoms^a

		HF			PBE			PBE0		
		$\Delta g_{ }$	Δg_{\perp}	Δg_{iso}	$\Delta g_{ }$	Δg_{\perp}	Δg_{iso}	$\Delta g_{ }$	Δg_{\perp}	Δg_{iso}
TiF ₃	LR	−1.2	−110.5	−74.1	−1.3	−43.2	−29.2	−1.5	−61.1	−41.3
	MA	−1.2	−110.6	−74.2	−1.2	−43.5	−29.4	−1.5	−61.4	−41.4
	LWA	−1.0	−81.7	−54.8	−0.9	−77.5	−51.9	−1.4	−94.7	−63.6
	exptl. ^{b,89}	−11.1	−111.1	−77.8	−11.1	−111.1	−77.8	−11.1	−111.1	−77.8
	exptl. ^{c,89}	−3.7	−123.7	−83.7	−3.7	−123.7	−83.7	−3.7	−123.7	−83.7
TcNCl ₄ [−]	LR	−41.4	−2.9	−15.7	39.6	3.7	15.7	28.0	0.5	9.6
	MA	−41.0	−3.4	−16.0	38.7	3.6	15.3	27.8	0.3	9.5
	LWA	67.1	−4.5	19.4	34.2	1.3	12.3	40.4	3.6	15.9
	exptl. ⁹⁰	6.0	−2.0	0.7	6.0	−2.0	0.7	6.0	−2.0	0.7
ReNCl ₄ [−]	LR	−184.7	−89.5	−121.2	11.6	−19.9	−9.4	−26.5	−24.1	−24.9
	MA	12.5	−28.7	−15.0	3.7	−21.2	−12.9	−28.9	−26.0	−26.9
	LWA	−74.0	−115.2	−101.5	−32.7	−75.2	−61.0	−30.4	−75.6	−60.5
	exptl. ⁹¹	−88.0	−57.0	−67.0	−88.0	−57.0	−67.0	−88.0	−57.0	−67.0
HgH	LR	0.0	−117.8	−78.6	0.0	−147.7	−98.5	0.0	−143.5	−95.7
	MA	−1.6	−142.7	−95.7	11.6	−186.1	−120.2	1.4	−176.0	−116.9
	LWA	−22.7	−243.6	−170.0	−28.9	−262.4	−184.6	−27.4	−262.3	−184.0
	exptl. ⁹²	−26.3	−174.3	−125.0	−26.3	−174.3	−125.0	−26.3	−174.3	−125.0
HgF	LR	0.0	−13.1	−8.8	−0.1	−25.8	−17.2	−0.1	−19.3	−12.9
	MA	−1.8	−19.6	−13.7	5.3	−34.3	−21.1	0.1	−25.5	−17.0
	LWA	−5.1	−47.2	−33.1	−13.4	−65.7	−48.3	−9.0	−56.9	−40.9
	exptl. ⁹²	−9.3	−41.3	−30.6	−9.3	−41.3	−30.6	−9.3	−41.3	−30.6

^aHF theory and DFT with the PBE and PBE0 functionals. ^bMeasurement in neon matrix. ^cArgon matrix.Table 5. *g* Shifts (in parts per thousand) for Molecule Set #2, with Main-Group and Transition Metal Atoms^a

		CAM-B3LYP			LC-PBE0		
		$\Delta g_{ }$	Δg_{\perp}	Δg_{iso}	$\Delta g_{ }$	Δg_{\perp}	Δg_{iso}
TiF ₃	LR	−1.3	−64.5	−43.4	−1.4	−81.8	−55.0
	MA	−1.3	−64.7	−43.6	−1.4	−82.0	−55.1
	LWA	−1.4	−94.6	−63.6	−2.3	−116.5	−78.4
	exptl. ^b	−11.1	−111.1	−77.8	−11.1	−111.1	−77.8
	exptl. ^c	−3.7	−123.7	−83.7	−3.7	−123.7	−83.7
TcNCl ₄ [−]	LR	23.6	0.2	8.0	13.2	−0.9	3.8
	MA	23.2	−0.7	7.2	13.1	−1.5	3.3
	LWA	41.8	5.0	17.2	41.0	4.9	16.9
	exptl.	6.0	−2.0	0.7	6.0	−2.0	0.7
ReNCl ₄ [−]	LR	−41.6	−24.8	−30.4	−59.2	−25.8	−36.9
	MA	−45.7	−34.4	−38.1	−60.1	−31.8	−41.3
	LWA	−35.7	−79.0	−64.6	−33.7	−76.4	−62.2
	exptl.	−88.0	−57.0	−67.0	−88.0	−57.0	−67.0
HgH	LR	0.0	−150.7	−100.5	0.0	−153.9	−102.6
	MA	−1.6	−179.4	−122.1	−2.2	−183.2	−124.6
	LWA	−29.0	−272.9	−191.6	−29.2	−279.4	−196.0
	exptl.	−26.3	−174.3	−125.0	−26.3	−174.3	−125.0
HgF	LR	−0.1	−15.1	−10.1	−0.1	−17.0	−11.3
	MA	−0.8	−19.3	−14.2	−1.1	−22.2	−15.9
	LWA	−8.8	−55.2	−39.8	−7.9	−56.5	−40.3
	exptl.	−9.3	−41.3	−30.6	−9.3	−41.3	−30.6

^aHybrid density functionals with range-separated exchange. ^bMeasurement in neon matrix. ^cArgon matrix.

degenerate set of half-occupied orbitals and the lowest unoccupied level), in particular for SiOH. We assert that in this case the *g* shifts become unreliable. In the spin-polarized calculations, the orbital gap is still very small (PBE: 0.02 eV). Systems with small HOMO–LUMO gaps are generally susceptible to perturbations. The LR data may be showing a breakdown because orbital energy gap denominators are explicitly present in the response equations.⁵⁵ We tentatively attribute the differences between LR and MA for the two

systems to such a numerical sensitivity in the LR calculations. If it were the case that higher-order SO effects become important because of a small HOMO–LUMO gap, this would be expected to lead to increased *g* shifts obtained from the MA approach instead. However, the data in Tables 2 and 3 exhibit the opposite trend.

4.4. Doublet Radicals with Transition Metals. Test set #2 comprises doublet radicals with light to heavy transition metal atoms (Ti, Tc, Re, Hg). The *g* shift data are collected in

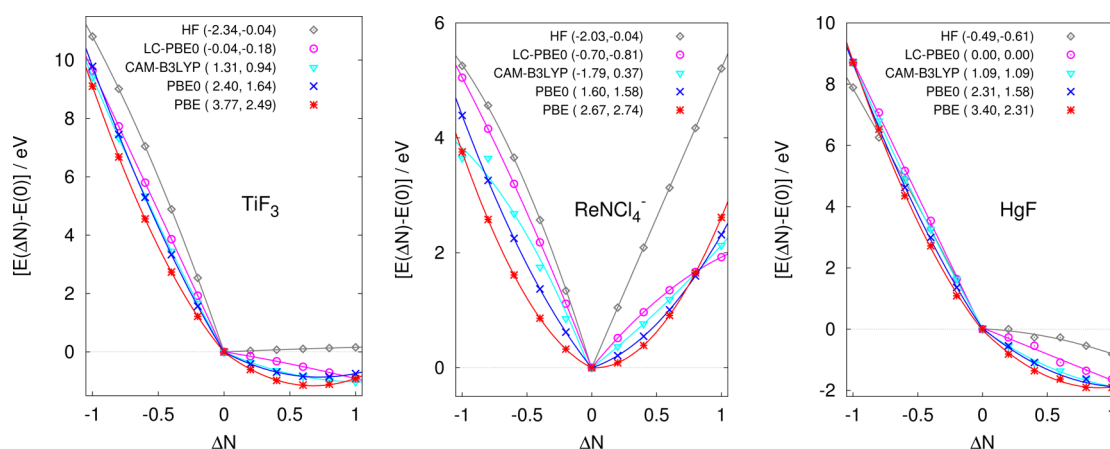


Figure 2. Left to right: DFT delocalization error for TiF_3 , ReNCl_4^- , and HgF . The plots show the change in ground state energy, $[E(\Delta N) - E(0)]$, in eV, of each system as a function of electron number N . Here, $\Delta N = N - N_0$ is relative to the electron number N_0 of the neutral species. Curvature measures listed in the plot legend are the coefficients of ΔN^2 of quadratic fits of $E(\Delta N)$ for the electron deficient and electron rich segments, respectively. Scalar ZORA data.

Tables 4 and 5. Experimental data are also included for comparison, although it is noted that an accurate computational model would require consideration of the environment of the molecule as it was studied experimentally (e.g., in a crystal or in a rare gas matrix).

Quantification of the importance of correlation, spin-polarization, the spin-dependent XC potential, and higher order SO effects in this test set becomes more complex as these different influences show interdependence. Differences in Δg tensor elements obtained from HF and DFT are significant. For the lighter metals Ti and Tc, the LR and MA approaches agree well. Differences are noteworthy for the systems with heavy atoms where higher order SO effects are expected to be of some importance. For instance, for HgH and HgF , a LR calculation based on a nonrelativistic electronic structure and with a nonrelativistic external-field perturbation operator would give a vanishing Δg_{\parallel} component because of the rotational symmetry (this has been pointed out numerous times in the literature; see ref 4 for a detailed discussion). The LR data in Tables 4 and 5 show that the present LR ZORA calculations also give negligible Δg_{\parallel} . The MA and LWA calculations produce nonvanishing Δg_{\parallel} components which must be attributed to higher-order SO effects. However, the Δg_{\parallel} are much smaller in magnitude than Δg_{\perp} .

For the 3d metal radical TiF_3 , MA and LR with HF orbitals provide the best results in comparison with experimental data, while PBE performs worst. We did not notice issues with small orbital gaps for this system, and therefore the comparison between MA and LWA can be used to demonstrate that spin-polarization is important for this system. We note in passing that this effect causes the ^{19}F hyperfine coupling constants to be negative; for a detailed analysis see ref 58. The experimental g tensor data obtained in different noble gas matrices show some variability, on the order of 10%, which means that the molecular environment has some effect as well. Perfect agreement with experiment should therefore not be expected for any of the calculations. On the other hand, the PBE results are clearly deficient. The g shift components get progressively better with the inclusion of nonlocal exact exchange in the functional (PBE0, CAM-B3LYP, LC-PBE0).

For the other systems, with the exception of HgH , the quality of the calculations is somewhat difficult to assess. We wondered if the poor performance of PBE for TiF_3 and the variability of

the data for HgF , TiNCl_4^- , and ReNCl_4^- is a manifestation of the DFT delocalization error.⁸⁷ Figure 2 provides an account of the extent of the delocalization error for TiF_3 , ReNCl_4^- , and HgF , based on calculations of the energy E with fractional electron numbers N going from the closed-shell cation via the neutral radical to the closed shell anion. Ideally, $E(N)$ should afford straight-line segments with slopes being equal to the negative ionization potential of the species with next higher integer N . The strongly positive curvatures for PBE are indicative of too much delocalization, which manifests itself in a too strongly covalent character of the metal–ligand bonds and unphysical delocalization of ligand lone-pair orbitals.⁹³ The negative curvature obtained with HF indicates that there is not enough delocalization. These findings are typical for pure density functionals versus HF theory. The hybrid functionals also give substantial delocalization errors for the two systems. For TiF_3 and HgF , the fully long-range corrected LC-PBE0 variant is reasonably close to the ideal behavior, with small curvatures of $E(N)$ in the segments between integer N (note that the HgF data have some numerical noise in the electron-rich segment). For ReNCl_4^- , the curvature with LC-PBE0 is remains sizable, and the negative curvature indicates that the functional behaves too HF-like. However, for the electron-deficient segment of $E(N)$, it performs best among the set of functionals. The steep slope of the HF energy for $\Delta N > 0$, which disagrees with all density functionals, indicates that the HF calculations are unreliable despite the good linear behavior in this segment. For the Re complex, a nonempirical functional tuning similar to one described in ref 94 may offer systematic improvements and lead to a more reliable calculation of its g shift. Overall, the MA calculations with the LC-PBE0 functional perform reasonably well for the different transition metal systems, and we consider this set of calculations as the most accurate for molecule set #2.

The inclusion of spin polarization in the calculations is apparently not beneficial in all cases. For example, the LWA calculations give closer agreement with experimental values for Δg_{\parallel} of HgH . However, the other tensor component and the isotropic average are consistently overestimated in the LWA calculations, irrespective of the functional. For HgF , the trend for Δg_{\parallel} is similar; viz., it appears to be underestimated by the spin-polarized MA calculations. The experimental Δg_{\perp} component is bracketed by the MA and LWA calculations

with the different density functionals. Among HF and the different functionals, HF performs best for HgH with the LWA approach, which we consider an example of the aforementioned interconnectedness of the various influences on the g shift which may provide varying degrees of error cancellations for different computational models. Interestingly, there is not a lot of variability of the MA data across the various density functionals for HgH. We comment further on this finding in section 4.5.

The Tc and Re complexes are challenging, since the relative magnitudes of the Δg_{\parallel} and Δg_{\perp} tensor components are sensitive to the fraction of exact exchange in the functional. Taking the Re complex as an example, the experimental Δg_{\parallel} component is more negative than Δg_{\perp} . All LWA calculations predict the opposite trend. The MA calculations with HF and PBE also give the wrong trend, but the situation improves considerably for the range-separated functionals. The influence of higher-order SO effects is noticeable for this system for the—presumably—best set of calculations, with LC-PBE0 (MA vs LR). The HF/LR calculation for this system is unreliable because of a large spin contamination ($\langle S^2 \rangle = 1.313$ instead of the expected value close to 0.75; for TcNCl_4^- , the HF value is 0.884 and therefore also indicates problems with the HF data for this system). The MA calculation is likely affected by the same issue. Here, the LWA approach performs somewhat better in comparison, because the quasi-restricted character of the calculation in some sense protects the system from converging to an unreasonable SCF solution. $\langle S^2 \rangle$ values for all systems from scalar ZORA calculations can be found in the Supporting Information.

For the 5d metal systems (HgH, HgF, ReNCl_4^-), the variational inclusion of SO coupling in the computations is required, since LR and MA g shifts deviate noticeably. In order to investigate this behavior further, additional MA calculations were performed for HgH. The ZORA spin–orbit operator integral matrices in the ground state SCF procedure were scaled by a factor λ such that $\lambda = 0$ corresponds to a scalar relativistic calculation, and $\lambda = 1$ to a full SO calculation. The spin-dependent operator matrices for the Zeeman Hamiltonian were not scaled. Figure 3 shows the unique Δg tensor components as a function of λ for HF and PBE calculations. For Δg_{\parallel} , the nonlinear nature is particularly evident; it has already been mentioned above that in the LR calculations this tensor component is suppressed because of the rotational symmetry. The LR and MA calculations yield more comparable

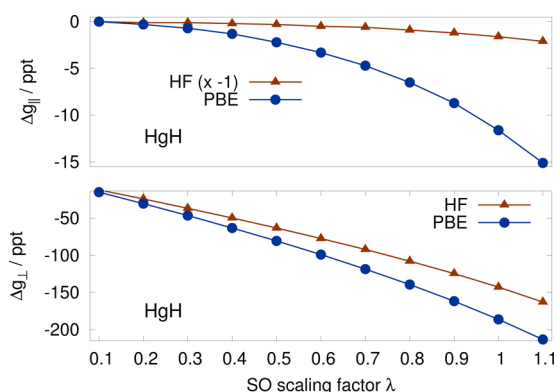


Figure 3. g shift tensor components of HgH calculated with the SO operator scaled by a factor λ . MA approach. See text for details.

Δg_{\perp} values, but with the LR calculations consistently underestimating its magnitude (consistent with Tables 4 and 5). Figure 3 nicely demonstrates the nonlinear behavior of this component, which leads to the larger magnitude of Δg_{\perp} in the variational SO calculations by around 30 ppt for the calculations with the range-separated hybrid functionals.

Hrobarik et al.⁴⁵ have previously studied the Tc and Re complex, along with related systems, and concluded that higher-order SO effects on g factors can be of significant importance. Our data corroborate this general statement for these and other systems. In Table 6, a comparison is made with

Table 6. Comparison of the Tc and Re Complex g Shifts (ppt) with Results Published by Hrobarik et al., ref 45^a

		BP			B3PW91		
		Δg_{\parallel}	Δg_{\perp}	Δg_{iso}	Δg_{\parallel}	Δg_{\perp}	Δg_{iso}
TcNCl_4^-	LR	40	4	16	32	1	11
	DKH-1comp ⁴⁵	40	5	17	34	3	13
	LWA	35	2	13	40	3	15
	DKH-2comp ⁴⁵	35	0	12	30	−3	8
	MA	39	4	16	32	1	11
	mDKS-4comp ⁴⁵	37	0	12			
ReNCl_4^-	LR	12	−19	−8	−18	−23	−21
	DKH-1comp ⁴⁵	−8	−17	−14	−47	−23	−31
	LWA	−32	−74	−60	−31	−75	−60
	DKH-2comp ⁴⁵	−46	−69	−61	−79	−75	−76
	MA	5	−20	−12	−21	−24	−23
	mDKS-4comp ⁴⁵	−54	−72	−66			

^aSee text for details.

the data published in ref 45 for the Tc and Re complex. The calculations of ref 45 utilized a LR approach similar to ours, but with the second-order DKH Hamiltonian (“DKH-1comp” in Table 6), along with a two-component DKH and a four-component method including higher-order SO effects mentioned in the Introduction (“DKH-2comp” and “mDKS-4comp,” respectively, in Table 6). The functionals used in ref 45 were the nonhybrid functional BP (or “BP86”), and the global hybrid B3PW91. Therefore, we performed additional calculations with these functionals for a direct comparison. We find that the ZORA/LR approach performs similarly to DKH-1comp (but not for the parallel component in the Re complex), and the ZORA/LWA approach performs similarly to DKH-2comp and mDKS-4comp. For TcNCl_4^- , the MA technique also produces comparable data. We already mentioned that higher order SO effects are not particularly significant for this system. There is a missing two-electron SO term in the present ZORA calculations (the spin–other-orbit term, SOO), which may be responsible for some of the differences between the results obtained with the different implementations. However, it is expected that the SOO terms rapidly decrease in relative importance to one-electron SO effects as the considered elements become heavier.^{95–97} On the basis of fully origin invariant GIAO calculations, Patchkovskii et al. found that SOO contributions to the g tensor are usually small.⁹⁸ There is therefore no pressing reason to expect major discrepancies between the different approaches for the Re system. Likewise,

Table 7. *g* Shifts (ppt) for Molecule Set #3, with Actinide Atoms^a

		PBE			PBE0			HF		
		LR	LWA	MA	LR	LWA	MA	LR	LWA	MA
NpF ₆	SCF ^b	−1710	−2434	−1707	−2209	−2735	−2033	−3331	−3074	−2841
(−2606) ¹⁰¹	PT2 ^c	−1733	−2458	−1731	−2248	−2762	−2069	−3420	−3096	−2910
UF ₆ [−]	SCF	−1872	−2721	−1908	−2311	−2907	−2127	−3278	−3063	−2648
(−2752) ¹⁰²	PT2	−1825	−2667	−1855	−2245	−2857	−2071	−3144	−3011	−2571
UCl ₆ [−]	SCF	−2351	−3077	−2444	−3083	−3231	−2777	−4929	−3373	−3466
(−3102) ¹⁰³	PT2	−2260	−3028	−2341	−2929	−3191	−2643	−4597	−3368	−3329

^aThe *g* tensors are isotropic, and therefore only the unique *g* shift is listed. HF, PBE, and PBE0 functionals. Experimental data in parentheses (converted from measured *g* factors with varying precision). ^bCASSCF geometry from ref 80. ^cCASPT2 geometry from ref 80.

Table 8. *g* Shifts (ppt) for Molecule Set #3, with Actinide Atoms^a

		CAM-B3LYP			LC-PBE0		
		LR	LWA	MA	LR	LWA	MA
NpF ₆	SCF	−2158	−2758	−1988	−2602	−2923	−2288
(−2606)	PT2	−2194	−2786	−2020	−2652	−2947	−2327
UF ₆ [−]	SCF	−2279	−2910	−2093	−2827	−3040	−2431
(−2752)	PT2	−2214	−2857	−2083	−2733	−2994	−2364
UCl ₆ [−]	SCF	−3026	−3267	−2726	−3953	−3322	−3185
(−3102)	PT2	−2877	−3228	−2596	−3735	−3292	−3037

^aHybrid functionals with range-separated exchange. See also Table 7.

ZORA is known to perform similarly well to DKH2 or four-component methods for valence shell properties in heavy element systems, i.e. the different relativistic approximations should perform comparably. Regarding the MA approach, by comparing the data for the Re complex in Tables 6 and 5, it is shown that the nonhybrid BP calculation produces *g*-shift tensor components that are roughly equivalent to the nonhybrid PBE functional. The results obtained with the B3PW91 hybrid are roughly equivalent to those from the PBE0 hybrid. As we have shown above, the Re complex *g* tensor is very sensitive to the choice of the functional, and much improved results are obtained with LC-PBE0 if agreement with experimental values is used as a guidance. A fair assessment of the different methods in comparison with experimental data would seem to require a larger range of functionals, in particular for the four-component relativistic approach.

4.5. Doublets with 5f Elements. The hexa-halide complexes of actinides in 5f^{II} oxidation states represent a suitable benchmark set for calculations due to their small size and the fact that their electronic structure and magnetic properties are quite well characterized. Scalar relativistic DFT calculations on NpF₆ have previously shown that the SOMO is predominantly the nonbonding 5f_{xyz} orbital (for ligand positions along the coordinate axes as shown in the graphical abstract). We consider here the octahedral systems NpF₆, UF₆[−], and UCl₆[−] (test set #3), which have isotropic *g* tensors. The experimentally determined *g* factors range from −0.6 for NpF₆ to −1.1 for UCl₆[−]. These systems therefore afford very large *g* shifts on the order of −2600 to −3100 ppt, driven by the strong SO coupling in the actinide 5f shell. Among computational EPR data for these and related systems available in the literature, we mention work by Case⁹⁹ and by Arratia-Pérez et al.¹⁰⁰ utilizing Dirac scattered-wave approaches within a local density approximation DFT framework, a multireference wave function-based study by Bolvin and Notter⁸⁰ using CASSCF and CASPT2 methods, and preliminary DFT studies performed by our group.^{55,88} The prior theoretical work confirmed the negative sign of the *g* factors for the complexes in

set #3. We adopted optimized CASSCF and CASPT2 geometries from ref 80 in order to investigate whether the *g* factors are sensitive to changes in the metal–ligand distance.

The results of the calculations are collected in Tables 7 and 8. The data for actinide systems exhibit a strong interdependence of the various factors that control the accuracy of the calculated *g* shifts, i.e., electron correlation, linear vs higher order SO effects, the treatment of spin polarization in the ground-state DFT calculations, and the treatment of spin polarization in the *g*-shift calculations (MA vs LWA). Compared to the strong variations with the functional, the effects from the different optimized geometries is secondary, albeit not completely negligible.

A priori, one would not expect the LR approach to come even close to the correct *g* shift magnitude for the actinide series. Case⁹⁹ pointed out that the SOMO in NpF₆ has *a*_{2u} symmetry in spin-free calculations (the aforementioned nonbonding 5f orbital) but *e*_{3u} double group symmetry in spin-orbit calculations. The latter, but not the former, can overlap with ligand p orbitals. SO coupling therefore causes important qualitative changes in the metal–ligand bonding. One would not expect a LR approach to succeed in such a situation. In a previous paper, we reported a LR ZORA implementation for *g* shifts in the ADF code⁸⁸ which uses Slater-type basis functions instead of the more common Gaussian-type functions (used in NWChem). Interestingly, for NpF₆ the ADF LR calculations gave comparable *g* shifts to those produced by the LWA implementation in ADF (for UF₆[−] and UCl₆[−], the LR data of ref 88 are likely unreliable for reasons noted below). However, in a subsequent DFT study utilizing our LR code in NWChem, the *g* shift of NpF₆ was calculated to be significantly smaller in magnitude,⁵⁵ although still sizable. Representative LR data are listed in Tables 7 and 8. We have subsequently attributed the discrepancy between the LR data obtained with the NWChem and ADF implementations to the lack of sufficiently high angular-momentum density fit basis functions in the ADF code.⁵⁵ This fit basis appears to have a strong impact on the LR *g* shifts while the LWA

approach is somewhat more robust. The present calculations for the three complexes and with additional functionals as well as HF theory support this assessment. The LWA results from ref 88, obtained with the PBE functional, were -2565 , -2803 , and -3122 , for NpF_6 , UF_6^- , and UCl_6^- , respectively, which are in reasonable agreement with the LWA PBE data from Table 7.

The importance of higher order SO effects is illustrated in Figure 4 where, similar to the HgF case discussed in section 4.4,

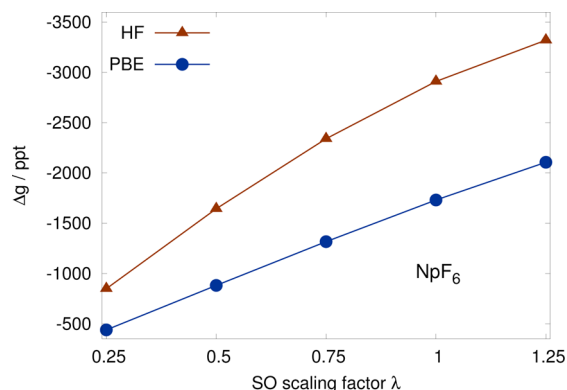


Figure 4. g shift of NpF_6 calculated with the SO operator scaled by a factor λ . MA approach. See text for details.

the SO operator integral matrix in MA calculations for NpF_6 has been scaled by a factor λ . The data obtained with the PBE functional exhibit a fairly linear behavior, whereas the HF data show a significant curvature indicating the importance of higher order SO effects on the g shift. Unlike for HgH , the higher order SO effects act to reduce the magnitude of the g shift. The lack of significant higher-order effects at the PBE level then explains why the results from LR and MA are so similar for this functional. At the HF level, as one would expect from the corresponding plot in Figure 4, the LR calculations strongly overestimate the magnitude of the g shift, not only for NpF_6 but also for the other two systems. Regarding the magnitude of higher order SO effects on the g shifts of the actinide systems in Tables 7 and 8, the hybrid density functionals exhibit a behavior ranging in between DFT and HF, with LC-PBE0 being closer to HF than functionals with less exact exchange.

In comparison with experimental values, and with the best CASSCF results from ref 80 (which are similar to the experimental data), LWA/PBE and MA/HF produce the most accurate g shifts. We attribute the fictitious equivalence of MA and LR for nonhybrid DFT due to effects from spin-polarization in the Kohn–Sham Fock operator. Thus, assuming that no serious errors in the code were left uncovered during the extensive testing phase, XC potentials from nonrelativistic functionals that only depend on the collinear spin densities appear not well suited for two-component relativistic spin-polarized magnetic property calculations for actinides. In the previous subsection, we observed that the calculated g shift tensor components for HgH exhibit relatively minor variations for the different density functionals. For this molecule, the differences between HF and DFT can therefore be attributed mainly to electron correlation. Incidentally, the scaled SO integral plots for HgH show comparable curvatures for the perpendicular g shift tensor component for HF and the PBE functional (Figure 3), much unlike the NpF_6 case. Therefore, for HgH , by including correlation on top of spin-polarization and higher order SO effects, the MA approach with DFT

provides the better results over HF theory. On the other hand, a (potentially) poor description of the XC potential in the two-component Fock operator appears to negate the effects of higher order SO effects for the actinide halide series. The amount of nonlocal exchange then becomes crucial for the MA approach. The LWA calculations do not include spin polarization, and here we find that with a nonhybrid spin-density functional such as PBE, the results are closer to experimental values than the MA results. Moreover, plots of the LWA g factor of NpF_6 calculated with HF and, in particular, PBE, as a function of a scaling factor λ applied to the SO operator exhibit strong nonlinear SO contributions to the g shift (Figure S1 in the Supporting Information). As exact exchange is mixed into the functional, and then going all the way to HF, some approximations inherent in the quasi spin-restricted LWA approach are exposed. The quasi-restricted calculations with HF and LC-PBE0 significantly overestimate the g shift magnitudes.

5. SUMMARY AND CONCLUSIONS

A comparison has been made between different relativistic methods to calculate g tensors of molecules with light atoms, transition metal complexes, and selected complexes with actinides, using density functional and HF theory. The g tensors were evaluated with a linear response (LR) method by which SO coupling is treated as a first-order perturbation, a spin-polarized approach (MA) including SO coupling variationally, and a quasi-restricted variational SO method previously devised by van Lenthe, van der Avoird, and Wormer (LWA). The MA and LWA methods were newly implemented for this work at the two-component hybrid DFT level, with support for functionals with range-separated exchange. Relativistic effects were treated by means of the ZORA approach. By means of using GIAO basis functions, a spurious dependence of the calculated data on the coordinate origin can be effectively eliminated. The results indicate that the origin dependence of g tensors of small molecules and small metal complexes is rather weak. The GIAO corrections become negligible with the basis sets used for the previous LR benchmark⁵⁵ when compared with other factors that influence the quality of the calculation, primarily approximations in the electronic structure model.

There are several important factors that determine the quality of the results, among those the treatment of electron correlation (DFT vs HF), consideration of spin polarization in the g tensor methodology, the treatment of spin-magnetization in DFT in conjunction with nonrelativistic spin-density functionals, and the treatment of SO coupling as a linear perturbation versus including SO coupling to higher orders.

Ground state calculations at a scalar relativistic level, and LR perturbation calculations, can be significantly less demanding computationally for large molecules than two-component relativistic calculations that include SO coupling in the ground state Hamiltonian. For calculations of g factors on systems that do not have heavy atoms (set #1), the LR approach is clearly adequate. The role of spin polarization also appears to be secondary for these neutral systems, and we did not find very large differences between uncorrelated HF calculations and DFT. For SiOH and SiSH , the quasi-restricted approach fails because of a vanishing HOMO–LUMO gap.

For the systems with heavier elements, the methods that include higher-order SO effects become increasingly more important as the nuclear charge of the heavy element increases,

and a spin-polarized approach is beneficial. For the Ti and Tc complexes, LR is still adequate. The interplay between the different influences and approximations that determine the accuracy of the calculation becomes very important for the heavy element systems. For example, for NpF₆ the higher-order SO effects are modulated by whether HF or a nonhybrid density functional is used for the calculation. An assessment of the performance of LR vs MA vs LWA is also affected by this interplay. For the actinide series, we find that the MA approach performs best with HF theory or with a density functional such as LR-PBE0 incorporating a lot of exact exchange. On the basis of the analysis of the data in section 4.5, the apparently good performance of LWA with nonhybrid functionals for the actinide complexes may be due to a compensation of errors, viz. the neglect of spin polarization in the method versus using a nonrelativistic spin-density functional in a two-component DFT calculation to account for the effects of the spin magnetization in the Fock operator. Keeping such caveats in mind, the MA approach overall performs reasonably well. We have also shown that this method performs fairly well for the transition metal complexes with functionals that afford a small delocalization error. The latter can be pronounced, as it was demonstrated explicitly for TiF₃, ReNCl₄[−], and HgF.

APPENDIX

In order to avoid a spurious origin dependence of the calculated *g* factors when using an incomplete basis set, gauge-including atomic orbitals (GIAOs, or London orbitals)^{64,65} can be employed. Given a standard atom-centered atomic orbital (AO) basis set { χ_μ }, the GIAO basis $\xi_\mu(\mathbf{B})$ is defined as

$$\xi_\mu(\mathbf{B}) = \chi_\mu \exp\left[\frac{i}{2}\mathbf{B} \cdot (\mathbf{r} \times \mathbf{R}_\mu)\right] \quad (20)$$

where \mathbf{R}_μ is the center of the AO basis function χ_μ . As a consequence, the partial derivatives $(\partial/\partial \mathbf{B}_u)\langle \Phi_i | \hat{F} | \Phi_j \rangle$ in the LWA approach and the derivatives $(\partial/\partial \mathbf{B}_u)\langle \varphi_i | \hat{F} | \varphi_j \rangle$ in eq 17 afford terms in addition to matrix elements of \hat{h}_u^Z . Let the functions ϕ_i and ϕ_j represent one of the φ_i^v of the MA approach or one of the Φ_i of the LWA scheme. The magnetic-field derivatives of the Fock matrix elements read

$$\begin{aligned} \frac{\partial}{\partial \mathbf{B}_u} \langle \phi_i(\mathbf{B}) | \hat{F} | \phi_j(\mathbf{B}) \rangle \\ = \langle \phi_i | \frac{\partial \hat{F}}{\partial \mathbf{B}_u} | \phi_j \rangle + \langle \frac{\partial \phi_i}{\partial \mathbf{B}_u} | \hat{F} | \phi_j \rangle + \langle \phi_i | \hat{F} | \frac{\partial \phi_j}{\partial \mathbf{B}_u} \rangle \end{aligned} \quad (21)$$

As noted previously, the derivatives imply $\mathbf{B} = 0$, i.e. field-free quantities unless explicitly noted otherwise. The new terms arising from the field-dependent basis are the last two terms on the right-hand side of eq 21 and, where applicable, two-electron exact-exchange integral GIAO derivatives in the exchange part of the Fock operator. The Coulomb and XC part of the Fock operator depend on the density, which is not perturbed by the magnetic field. In the GIAO basis, the partial derivatives of the Kohn–Sham spinors with respect to the magnetic field read

$$\frac{\partial \phi_i}{\partial \mathbf{B}_u} = \sum_k \phi_k A_{ki}^u + \sum_\mu \left[\frac{i}{2} (\mathbf{r} \times \mathbf{R}_\mu)_u \right] \chi_\mu \begin{pmatrix} C_{\mu i}^\alpha \\ C_{\mu i}^\beta \end{pmatrix} \quad (22)$$

Here, the A_{ki}^u are MO mixing coefficients used to preserve the MO orthonormality, $\mathbf{C}^\dagger \mathbf{S} \mathbf{C} = \mathbf{1}$, to first order in the field. In eq 22, the index *k* runs over all occupied (occ) MOs, i.e. $i, k \in \text{occ}$.

Further, the $C_{\mu i}^v$ are the two-component MO coefficients for $\mathbf{B} = 0$. In order to get the full magnetic field response, one also needs the A_{ai}^u where the index *a* runs over the set of unoccupied orbitals, which describes the perturbation of the occupied orbitals due to the implicit field-dependence of the MO coefficients. As noted in section 2.3, here we only need to consider terms that depend explicitly on the magnetic field. For the occ–occ block of the A^u matrices, we adopt the usual choice

$$A_{ki}^u = -\frac{1}{2} S_{ki}^u \quad (23)$$

which ensures $(\partial/\partial \mathbf{B}_u) \mathbf{C}^\dagger \mathbf{S} \mathbf{C} = 0$ in conjunction with eq 22. In the previous equation,

$$S_{ki}^u = \frac{i}{2} \sum_{\mu\nu} C_{\mu k}^\dagger \langle \chi_\mu | [\mathbf{r} \times (\mathbf{R}_\nu - \mathbf{R}_\mu)]_u | \chi_\nu \rangle C_{\nu i} \quad (24)$$

is the B_u derivative of an element of the GIAO overlap matrix \mathbf{S} , transformed to the set of unperturbed MOs. As elsewhere, $C_{\mu i}^\dagger \dots C_{\nu j}$ notation implies summation over spin indices for scalar or two-component operator matrix elements.

Substitution of eq 22 in eq 21 gives for the last two terms of eq 21

$$\begin{aligned} \langle \frac{\partial \phi_i}{\partial \mathbf{B}_u} | \hat{F} | \phi_j \rangle + \langle \phi_i | \hat{F} | \frac{\partial \phi_j}{\partial \mathbf{B}_u} \rangle \\ = -\frac{1}{2} S_{ij}^u (\epsilon_j + \epsilon_i) + \sum_{\mu\nu} C_{\mu i}^\dagger \langle \chi_\mu | -\frac{i}{2} (\mathbf{r} \times \mathbf{R}_\mu)_u \hat{F} | \chi_\nu \rangle C_{\nu j} \\ + \sum_{\mu\nu} C_{\mu i}^\dagger \langle \chi_\mu | \hat{F} | \frac{i}{2} (\mathbf{r} \times \mathbf{R}_\nu)_u | \chi_\nu \rangle C_{\nu j} \end{aligned} \quad (25)$$

where (without field) $\langle \phi_k | \hat{F} | \phi_l \rangle = \epsilon_j \delta_{kl}$, $\langle \phi_l | \hat{F} | \phi_k \rangle = \epsilon_l \delta_{lk}$, and $S_{ji}^{u*} = S_{ij}^u$ have been used. The ϵ_i are the unperturbed orbital energies. In the LWA and the MA approaches, the two orbitals involved in the matrix elements are either identical or energetically degenerate, and the first term on the right-hand side of eq 25 then reads $-S_{ij}^u \epsilon_i$ or $-S_{ij}^u \epsilon_j$.

In order to demonstrate the origin invariance of the working expressions, it is convenient to rewrite the last term on the right-hand side of eq 25. The derivatives in the one-electron ZORA part of \hat{F} do not commute with \mathbf{r} . For the field-free ZORA operator, the commutator reads

$$[\hat{h}, \mathbf{r}] = -\frac{i}{2} (\hat{\mathbf{p}} \mathcal{K} + \mathcal{K} \hat{\mathbf{p}}) + \frac{1}{2} \{ \boldsymbol{\sigma} \times \hat{\mathbf{p}} \mathcal{K} \} \quad (26)$$

where the spin-dependent part originates from the ZORA SO term. The same notation {...} as in eq 8 is used to indicate derivatives that are only taken within the operator. Using eq 26 in the last term of eq 25, and considering that the derivatives of \mathbf{R}_ν vanish, gives

$$\begin{aligned} \langle \chi_\mu | -\frac{i}{2} (\mathbf{r} \times \mathbf{R}_\mu)_u \hat{F} | \chi_\nu \rangle + \langle \chi_\mu | \hat{F} | \frac{i}{2} (\mathbf{r} \times \mathbf{R}_\nu)_u | \chi_\nu \rangle \\ = \frac{i}{2} \langle \chi_\mu | [\mathbf{r} \times (\mathbf{R}_\nu - \mathbf{R}_\mu)]_u \hat{F} | \chi_\nu \rangle \\ - \frac{1}{4} \langle \chi_\mu | [\mathbf{R}_\nu \times (\hat{\mathbf{p}} \mathcal{K} + \mathcal{K} \hat{\mathbf{p}})]_u | \chi_\nu \rangle \\ - \frac{1}{4} \left[\langle \chi_\mu | \sigma_u \{ \nabla \cdot \mathcal{K} \mathbf{R}_\nu \} - \boldsymbol{\sigma} \cdot \{ \nabla_u \mathcal{K} \mathbf{R}_\nu \} | \chi_\nu \rangle \right] \end{aligned} \quad (27)$$

The last two terms in eq 27 are equivalent to AO matrix elements of \hat{h}_u^Z of eq 9, but with the electron coordinate \mathbf{r}

replaced by $-\mathbf{R}_\nu$. Using $\mathbf{r}_\nu = \mathbf{r} - \mathbf{R}_\nu$, the Fock matrix element derivative in eq 21 can therefore be recast as follows:

$$\begin{aligned} \frac{\partial}{\partial B_u} \langle \phi_i(\mathbf{B}) | \hat{F}(\mathbf{B}) | \phi_j(\mathbf{B}) \rangle \\ = -\frac{1}{2} S_{ij}^u (\varepsilon_j + \varepsilon_i) + \frac{1}{4} \sum_{\mu\nu} C_{\mu i}^\dagger \left[\langle \chi_\mu | [\mathbf{r}_\nu \times (\hat{\mathbf{p}}\mathcal{K} + \mathcal{K}\hat{\mathbf{p}})]_u \right. \\ \left. + \sigma_u \{ \nabla \cdot \mathcal{K} \mathbf{r}_\nu \} - \sigma \cdot \{ \nabla_u \mathcal{K} \mathbf{r}_\nu \} | \chi_\nu \rangle \right] C_{\nu j} \\ + \frac{i}{2} \sum_{\mu\nu} C_{\mu i}^\dagger \langle \chi_\mu | [\mathbf{r} \times (\mathbf{R}_\nu - \mathbf{R}_\mu)]_u \hat{F} | \chi_\nu \rangle C_{\nu j} \end{aligned} \quad (28)$$

As previously, summation over spin indices is implied. In hybrid DFT calculations, the expression additionally includes GIAO two-electron exchange integral derivatives from $\partial \hat{F} / \partial B_u$ in the first term on the right-hand side of eq 21. In the present implementation, these additional terms are omitted because of the overall weak origin dependence found in the calculations, as discussed in section 4.1.

Consider now the behavior of the last expression if the coordinate origin is shifted such that $\mathbf{r} \rightarrow \mathbf{r} + \mathbf{a}$, with \mathbf{a} being some constant vector. With the GIAO basis set, there must be a cancellation of any additional terms depending on \mathbf{a} such as to render eq 28 origin invariant. The expression contains operators that are defined relative to atomic centers within the molecule (via \mathbf{r}_ν), and therefore each of these terms is already invariant with respect to an origin shift. For $\mathbf{r} \rightarrow \mathbf{r} + \mathbf{a}$, the last term on the right-hand side of eq 28 acquires an additional contribution

$$\frac{i}{2} \sum_{\mu\nu} [\mathbf{a} \times (\mathbf{R}_\nu - \mathbf{R}_\mu)]_u C_{\mu i}^\dagger \langle \chi_\mu | \hat{F} | \chi_\nu \rangle C_{\nu j} \quad (29)$$

where we took $[\mathbf{a} \times (\mathbf{R}_\nu - \mathbf{R}_\mu)]_u$ out of the AO matrix element because it is a constant. The origin shifts for the atomic centers $\mathbf{R}_\mu, \mathbf{R}_\nu$ cancel in the expression. Let the parts of the MOs that are centered on a given nucleus A be given by

$$\phi_i^A = \sum_{\mu \text{ on } A} \chi_\mu \begin{pmatrix} C_{\mu i}^\alpha \\ C_{\mu i}^\beta \end{pmatrix} \quad (30)$$

The basis functions in expression 29 can then be grouped by different nuclear centers, to give

$$\frac{i}{2} \sum_A [\mathbf{a} \times \mathbf{R}_A]_u \langle \phi_i | \hat{F} | \phi_j^A \rangle - \frac{i}{2} \sum_A [\mathbf{a} \times \mathbf{R}_A]_u \langle \phi_i^A | \hat{F} | \phi_j \rangle \quad (31)$$

In the same fashion, the additional terms obtained from the origin shift $\mathbf{r} \rightarrow \mathbf{r} + \mathbf{a}$ in the S_{ij}^u term in eq 28 can be written as

$$-\varepsilon_j \frac{i}{2} \sum_A [\mathbf{a} \times \mathbf{R}_A]_u \langle \phi_i | \phi_j^A \rangle + \varepsilon_j \frac{i}{2} \sum_A [\mathbf{a} \times \mathbf{R}_A]_u \langle \phi_i^A | \phi_j \rangle \quad (32)$$

assuming $\varepsilon_i = \varepsilon_j$, which is the case for the LWA and MA approaches. From the field-free KS equation in matrix form, one can extract identities of the type

$$\begin{aligned} \langle \phi_i^A | \hat{F} | \phi_j \rangle &= \varepsilon_j \langle \phi_i^A | \phi_j \rangle \\ \langle \phi_i | \hat{F} | \phi_j^A \rangle &= \varepsilon_i \langle \phi_i | \phi_j^A \rangle \end{aligned} \quad (33)$$

There is no assumption made that the KS equation $\hat{F}\phi_j = \phi_j \varepsilon_j$ is satisfied point-wise in space, which would require a complete basis, but rather in its integrated form in the basis set approximation as written in eq 3. The expressions in eq 33 are sufficient to show that the individual terms for each nuclear center A in eqs 31 and 32 cancel identically. Therefore, the matrix element derivatives in eq 28 needed for the MA and LWA approaches are confirmed to be origin invariant.

In the code, GIAO functionality that was developed as part of the NMR and LR g shift implementations in NWChem^{55,66,67} is used to calculate GIAO terms involving V_{ext} as well as two-electron terms in the expression analytically. The remaining terms are evaluated by numerical integration. The two-component ZORA operator matrices were implemented in a form utilizing eq 25 and the unmodified Zeeman operator derivative of eq 9. From a numerical perspective, expression 28 should give identical results irrespective of the quality of the numerical grid. However, it is easier to prove the origin invariance based on eq 28. For additional details about the evaluation of matrix elements related to the ZORA Zeeman and SO operators as well as GIAO contributions involving these operators in NWChem, see also ref 55.

■ ASSOCIATED CONTENT

● Supporting Information

Additional calculated data for LWA/PBE showing the weak origin dependence of the g shifts with the basis sets used to calculate the results of sections 4.2–4.5 (Tables S1–S3). \hat{S}^2 expectation values calculated with spin-unrestricted scalar ZORA (Table S4). Additional results for NpF₆ similar to those shown in Figure 4 but calculated with the LWA approach (Figure S1). This material is available free of charge via the Internet at <http://pubs.acs.org>.

■ AUTHOR INFORMATION

Corresponding Author

*E-mail: jochena@buffalo.edu.

Notes

The authors declare no competing financial interest.

■ ACKNOWLEDGMENTS

This research was funded by the U.S. Department of Energy, Office of Basic Energy Sciences, Heavy Element Chemistry program, under grant DE-FG02-09ER16066. We further acknowledge support by the Center for Computational Research (CCR) at the University at Buffalo. J.A. thanks Professor Christoph van Wüllen for helpful discussions during the 2012 Mariapfarr relativistic quantum chemistry workshop and at the 2012 Chemistry and Physics of the Heavy Elements symposium in Santa Fe. Further, J.A. thanks Dr. Erik van Lenthe and Dr. Serguei Patchkovskii for stimulating discussions on the topic of calculating EPR parameters. We acknowledge an ongoing collaboration with Dr. Niranjana Govind (Pacific Northwest National Laboratory) on various improvements of the NWChem spin-orbit DFT module.

■ REFERENCES

- (1) Dyall, K. G.; Faegri, K., Jr. *Relativistic Quantum Chemistry*; Oxford University Press: New York, 2007.
- (2) Reiher, M.; Wolf, A. *Relativistic Quantum Chemistry. the Fundamental Theory of Molecular Science*; Wiley-VCH: Weinheim, Germany, 2009.

- (3) Atherton, N. M. *Principles of Electron Spin Resonance*, Ellis Horwood Series in Physical Chemistry; Prentice Hall: New York, 1993; p 38.
- (4) Patchkovskii, S.; Schreckenbach, G. Calculation of EPR g-tensors with density functional theory. In *Calculation of NMR and EPR Parameters. Theory and Applications*; Kaupp, M.; Bühl, M.; Malkin, V. G., Eds.; Wiley-VCH: Weinheim, Germany, 2004; pp 505–532.
- (5) Abragam, A.; Bleaney, B. *Electron Paramagnetic Resonance of Transition Ions*; Clarendon Press: Oxford, U. K., 1970.
- (6) Stone, A. *Mol. Phys.* **1963**, *6*, 509–515.
- (7) Keijzers, C. P.; De Vries, H. J. M.; van der Avoird, A. *Inorg. Chem.* **1972**, *11*, 1338–1343.
- (8) Mishra, K. C.; Mishra, S. K.; Roy, J. N.; Ahmad, S.; Das, T. P. *J. Am. Chem. Soc.* **1985**, *107*, 7898–7904.
- (9) Roy, J. N.; Mishra, K. C.; Mishra, S. K.; Das, T. P. *J. Phys. Chem.* **1989**, *93*, 194–200.
- (10) Morikawa, T.; Kikuchi, O.; Someno, K. *Theor. Chem. Acc.* **1971**, *22*, 224–228.
- (11) Chuvylkin, N.; Zhidomirov, G.; Umansky, I. *Chem. Phys. Lett.* **1975**, *33*, 576–578.
- (12) Hudson, A.; Treweek, R. F.; Wiffen, J. T. *Theor. Chem. Acc.* **1975**, *38*, 355–358.
- (13) Angstl, R. *Chem. Phys.* **1989**, *132*, 435–442.
- (14) Chuvylkin, N.; Zhidomirov, G. *Mol. Phys.* **1973**, *25*, 1233–1235.
- (15) Lin, M.; Lunsford, J. J. *Magn. Reson.* **1978**, *29*, 151–157.
- (16) Zhidomirov, G.; Kabankin, A. J. *Magn. Reson.* **1975**, *19*, 47–50.
- (17) Pryce, M. H. L. *Proc. Phys. Soc. A* **1950**, *63*, 25.
- (18) Törring, J. T.; Un, S.; Knüpling, M.; Plato, M.; Möbius, K. *J. Chem. Phys.* **1997**, *107*, 3905–3913.
- (19) Montgolfier, P.; Harriman, J. E. *J. Chem. Phys.* **1971**, *55*, 5262–5269.
- (20) Stone, A. J. *Proc. R. Soc. London, Ser. A* **1963**, *271*, 424–434.
- (21) Tipples, H. H. *Phys. Rev.* **1967**, *160*, 343–345.
- (22) Atkins, P.; Jamieson, A. *Mol. Phys.* **1968**, *14*, 425–431.
- (23) Moores, W. H.; McWeeny, R. *Proc. R. Soc. London, Ser. A* **1973**, *332*, 365.
- (24) Lushington, G. H.; Grein, F. *J. Chem. Phys.* **1997**, *106*, 3292–3300.
- (25) Bolvin, H. *ChemPhysChem* **2006**, *7*, 1575–1589.
- (26) Gerloch, M.; McMeeking, R. F. *J. Chem. Soc., Dalton Trans.* **1975**, 2443–2451.
- (27) Pierloot, K.; Delabie, A.; Groothaert, M. H.; Schoonheydt, R. A. *Phys. Chem. Chem. Phys.* **2001**, *3*, 2174–2183.
- (28) Chibotaru, L. F.; Hendrickx, M. F. A.; Clima, S.; Larionova, J.; Ceulemans, A. *J. Phys. Chem. A* **2005**, *109*, 7251–7257.
- (29) Geurts, P. J. M.; Bouten, P. C. P.; van der Avoird, A. *J. Chem. Phys.* **1980**, *73*, 1306–1312.
- (30) Belanzoni, P.; Baerends, E. J.; van Asselt, S.; Langewen, P. B. *J. Phys. Chem.* **1995**, *99*, 13094–13102.
- (31) Schreckenbach, G.; Ziegler, T. *J. Phys. Chem. A* **1997**, *101*, 3388–3399.
- (32) Malkina, O. L.; Vaara, J.; Schimmelpennig, B.; Munzarova, M.; Malkin, V. G.; Kaupp, M. *J. Am. Chem. Soc.* **2000**, *122*, 9206–9218.
- (33) Patchkovskii, S.; Ziegler, T. *J. Chem. Phys.* **1999**, *111*, 5730–5740.
- (34) Autschbach, J.; Seth, M.; Ziegler, T. *J. Chem. Phys.* **2007**, *126*, 174103–5.
- (35) Neese, F. *J. Chem. Phys.* **2001**, *115*, 11080–11096.
- (36) Rinkevicius, Z.; Telyatnyk, L.; Salek, P.; Vahtras, O.; Ågren, H. *J. Chem. Phys.* **2003**, *119*, 10489–10496.
- (37) Rinkevicius, Z.; de Almeida, K. J.; Vahtras, O. *J. Chem. Phys.* **2008**, *129*, 064109.
- (38) Fernandez, B.; Jørgensen, P.; Byberg, J.; Olsen, J.; Helgaker, T.; Jensen, H. J. A. *J. Chem. Phys.* **1992**, *97*, 3412–3419.
- (39) Gilka, N.; Tatchen, J.; Marian, C. *Chem. Phys.* **2008**, *343*, 258–269.
- (40) Neese, F. *Chem. Phys. Lett.* **2003**, *380*, 721–728.
- (41) van Lenthe, E.; Wormer, P. E. S.; van der Avoird, A. *J. Chem. Phys.* **1997**, *107*, 2488–2498.
- (42) Neyman, K. M.; Ganyushin, D. I.; Matveev, A. V.; Nasluzov, V. A. *J. Phys. Chem. A* **2002**, *106*, 5022–5030.
- (43) Jayatilaka, D. *J. Chem. Phys.* **1998**, *108*, 7587–7594.
- (44) Malkin, I.; Malkina, O. L.; Malkin, V. G.; Kaupp, M. *J. Chem. Phys.* **2005**, *123*, 244103–16.
- (45) Hrobarik, P.; Repisky, M.; Komorovsky, S.; Hrobarikova, V.; Kaupp, M. *Theor. Chem. Acc.* **2011**, *129*, 715–725.
- (46) Liu, W. *Mol. Phys.* **2010**, *108*, 1679–1706.
- (47) Saue, T. *ChemPhysChem* **2011**, *12*, 3077–3094.
- (48) Pyykkö, P. *Annu. Rev. Phys. Chem.* **2012**, *63*, 45–64.
- (49) Autschbach, J. *J. Chem. Phys.* **2012**, *136*, 150902–15.
- (50) van Wüllen, C. *Relativistic Density Functional Theory. In Relativistic Methods for Chemists*; Barysz, M.; Ishikawa, Y., Eds.; Springer: Dordrecht, The Netherlands, 2010; Vol. 10, pp 191–214.
- (51) van Lenthe, E. *The ZORA Equation*, Thesis, Vrije Universiteit Amsterdam, The Netherlands, 1996.
- (52) Wolff, S. K.; Ziegler, T.; van Lenthe, E.; Baerends, E. J. *J. Chem. Phys.* **1999**, *110*, 7689–7698.
- (53) Autschbach, J.; Ziegler, T. *J. Chem. Phys.* **2000**, *113*, 9410–9418.
- (54) Nichols, P.; Govind, N.; Bylaska, E. J.; de Jong, W. A. *J. Chem. Theory Comput.* **2009**, *5*, 491–499.
- (55) Aquino, F.; Govind, N.; Autschbach, J. *J. Chem. Theory Comput.* **2011**, *7*, 3278–3292.
- (56) Ziegler, T.; Seth, M.; Krykunov, M.; Autschbach, J.; Wang, F. *J. Chem. Phys.* **2009**, *130*, 154102–8.
- (57) Aquino, F.; Govind, N.; Autschbach, J. *J. Chem. Theory Comput.* **2010**, *6*, 2669–2686.
- (58) Aquino, F.; Pritchard, B.; Autschbach, J. *J. Chem. Theory Comput.* **2012**, *8*, 598–609.
- (59) Valiev, M.; Bylaska, E. J.; Govind, N.; Kowalski, K.; Straatsma, T. P.; Dam, H. J. V.; Wang, D.; Nieplocha, J.; Apra, E.; Windus, T. L.; de Jong, W. A. *Comput. Phys. Commun.* **2010**, *181*, 1477–1489.
- (60) van Wüllen, C. *J. Chem. Phys.* **2009**, *130*, 194109–14.
- (61) Schmitt, S.; Jost, P.; van Wüllen, C. *J. Chem. Phys.* **2011**, *134*, 194113–11.
- (62) van Wüllen, C. Mariaparr 2012 Workshop Lecture Notes, pt. 3. <http://www.uni-graz.at/tchwww/mariaparr12/vanWuellen.zip> (accessed 12/2012).
- (63) Autschbach, J.; Zheng, S. *Annu. Rep. NMR Spectrosc.* **2009**, *67*, 1–95.
- (64) London, F. *J. Phys. Radium* **1937**, *8*, 397–409.
- (65) Ditchfield, R. *Mol. Phys.* **1974**, *27*, 789–807.
- (66) Dupuis, M. *Comput. Phys. Commun.* **2001**, *134*, 150–166.
- (67) Srebro, B.; Govind, N.; de Jong, W.; Autschbach, J. *J. Phys. Chem. A* **2011**, *115*, 10930–10949.
- (68) Kutzelnigg, W.; Fleischer, U.; Schindler, M. The IGLO-Method: Ab Initio Calculation and Interpretation of NMR Chemical Shifts and Magnetic Susceptibilities. In *NMR Basic Principles and Progress*; Diehl, P.; Fluck, E.; Gunther, H.; Kosfeld, R.; Seelig, J., Eds.; Springer-Verlag: Heidelberg, Germany, 1990; Vol. 23, pp 165–262.
- (69) Roos, B. O.; Lindh, R.; Malmqvist, P.; Veryazov, V.; Widmark, P. *J. Phys. Chem. A* **2005**, *109*, 6575–6579.
- (70) Roos, B. O.; Lindh, R.; Malmqvist, P.; Veryazov, V.; Widmark, P.-O. *Chem. Phys. Lett.* **2005**, *409*, 295–299.
- (71) Autschbach, J.; Peng, D.; Reiher, M. *J. Chem. Theory Comput.* **2012**, *8*, 4239–4248.
- (72) Becke, A. D. *Phys. Rev. A* **1988**, *38*, 3098–3100.
- (73) Perdew, J. P. *Phys. Rev. B* **1986**, *33*, 8822–8824.
- (74) Becke, A. D. *J. Chem. Phys.* **1993**, *98*, 5648–5652.
- (75) Perdew, J. P.; Burke, K.; Ernzerhof, M. *Phys. Rev. Lett.* **1997**, *78*, 1396–1396.
- (76) Adamo, C.; Barone, V. *J. Chem. Phys.* **1999**, *110*, 6158–6170.
- (77) Yanai, T.; Tew, D. P.; Handy, N. C. *Chem. Phys. Lett.* **2004**, *393*, 51–57.
- (78) Rohrdanz, M. A.; Herbert, J. M. *J. Chem. Phys.* **2008**, *129*, 034107-9.
- (79) Baerends, E. J.; Ziegler, T.; Autschbach, J.; Bashford, D.; Bérces, A.; Bickelhaupt, F. M.; Bo, C.; Boerrigter, P. M.; Cavallo, L.; Chong, D. P.; Deng, L.; Dickson, R. M.; Ellis, D. E.; van Faassen, M.; Fan, L.;

Fischer, T. H.; Fonseca Guerra, C.; Ghysels, A.; Giammona, A.; van Gisbergen, S. J. A.; Götz, A. W.; Groeneveld, J. A.; Gritsenko, O. V.; Grüning, M.; Gusarov, S.; Harris, F. E.; van den Hoek, P.; Jacob, C. R.; Jacobsen, H.; Jensen, L.; Kaminski, J. W.; van Kessel, G.; Kootstra, F.; Kovalenko, A.; Krykunov, M. V.; van Lenthe, E.; McCormack, D. A.; Michalak, A.; Mitoraj, M.; Neugebauer, J.; Nicu, V. P.; Noodleman, L.; Osinga, V. P.; Patchkovskii, S.; Philipsen, P. H. T.; Post, D.; Pye, C. C.; Ravenek, W.; Rodríguez, J. I.; Ros, P.; Schipper, P. R. T.; Schreckenbach, G.; Seldenthuis, J. S.; Seth, M.; Snijders, J. G.; Solà, M.; Swart, M.; Swerhone, D.; te Velde, G.; Vernooijs, P.; Versluis, L.; Visscher, L.; Visser, O.; Wang, F.; Wesolowski, T. A.; van Wezenbeek, E. M.; Wiesenekker, G.; Wolff, S. K.; Woo, T. K.; Yakovlev, A. L. *Amsterdam Density Functional*; SCM, Theoretical Chemistry, Vrije Universiteit: Amsterdam, The Netherlands. URL: <http://www.scm.com> (accessed Dec. 2012).

- (80) Notter, F.-P.; Bolvin, H. *J. Chem. Phys.* **2009**, *130*, 184310.
- (81) Baldas, J.; Boas, J. F.; Bonnyman, J.; Williams, G. A. *J. Chem. Soc., Dalton Trans.* **1984**, 2395–2400.
- (82) Liese, W.; Dehnicke, K.; Rogers, R. D.; Shakir, R.; Atwood, J. L. *J. Chem. Soc., Dalton Trans.* **1981**, 1061–1063.
- (83) Helgaker, T.; Jørgensen, P. *J. Chem. Phys.* **1991**, *95*, 2595–2601.
- (84) Krykunov, M.; Autschbach, J. *J. Chem. Phys.* **2007**, *126*, 024101–12.
- (85) Gauss, J. Molecular Properties. In *Modern Methods and Algorithms of Quantum Chemistry*; Grotendorst, J., Ed.; John von Neumann Institute for Computing: Jülich, Germany, 2000; Vol. 3, pp 541–592.
- (86) Pantazis, D. A.; Chen, X.-Y.; Landis, C. R.; Neese, F. *J. Chem. Theory Comput.* **2008**, *4*, 908–919.
- (87) Cohen, A. J.; Mori-Sánchez, P.; Yang, W. *Science* **2008**, *321*, 792–794.
- (88) Autschbach, J.; Pritchard, B. *Theor. Chem. Acc.* **2011**, *129*, 453–466.
- (89) De Vore, T. C.; Weltner, W. *J. Am. Chem. Soc.* **1977**, *99*, 4700–4703.
- (90) Kirmse, R.; Khler, K.; Abram, U.; Bttcher, R.; Goli, L.; Boer, E. *J. Chem. Phys.* **1990**, *143*, 75–82.
- (91) Lack, G. M.; Gibson, J. F. *J. Mol. Struct.* **1978**, *46*, 299–306.
- (92) Weltner, W., Jr. *Magnetic Atoms and Molecules*; Dover Publications, Inc.: New York, 1983.
- (93) Pritchard, B.; Autschbach, J. *Inorg. Chem.* **2012**, *51*, 8340–8351.
- (94) Srebro, M.; Autschbach, J. *J. Phys. Chem. Lett.* **2012**, *3*, 576–581.
- (95) Okada, S.; Shinada, M.; Matsuoka, O. *J. Chem. Phys.* **1990**, *93*, 5013–5019.
- (96) Ishikawa, Y.; Nakajima, T.; Hada, M.; Nakatsuji, H. *Chem. Phys. Lett.* **1998**, *283*, 119–124.
- (97) Vaara, J.; Ruud, K.; Vahtras, O.; Ågren, H.; Jokisaari, J. *J. Chem. Phys.* **1998**, *109*, 1212–1222.
- (98) Patchkovskii, S.; Strong, R. T.; Pickard, C. J.; Un, S. *J. Chem. Phys.* **2005**, *122*, 214101–9.
- (99) Case, D. A. *J. Chem. Phys.* **1985**, *83*, 5792–5796.
- (100) Arratia-Pérez, R.; Hernandez-Acevedo, L.; Malli, G. L. *J. Chem. Phys.* **2004**, *121*, 7743–7747.
- (101) Hutchison, C. A., Jr.; Weinstock, B. *J. Chem. Phys.* **1960**, *32*, 56–61.
- (102) Rigny, P.; Plurien, P. *J. Phys. Chem. Solids* **1967**, *28*, 2589–2595.
- (103) Selbin, J.; Ortego, J. D.; Gritzner, G. *Inorg. Chem.* **1968**, *7*, 976–982.
- (104) Chibotaru, L. F.; Ungur, L. *J. Chem. Phys.* **2012**, *137*, 064112.